Boron Isotopic Composition of the Subcontinental Lithospheric Mantle

by

Meghan R. Guild

A Thesis Presented in Partial Fulfillment of the
Requirements for the Degree
Master of Science

Approved June 2014 by the
Graduate Supervisory Committee:

Richard L. Hervig, Chair
David R. Bell
Allen McNamara

ARIZONA STATE UNIVERSITY

December 2014

ABSTRACT

Boron concentrations and isotopic composition of phlogopite mica, amphibole, and selected coexisting anhydrous phases in mantle-derived xenoliths from the Kaapvaal Craton were measured by secondary ion mass spectrometry in an effort to better understand the B isotope geochemistry of the subcontinental lithospheric mantle (SCLM) and its implications for the global geochemical cycle of B in the mantle. These samples display a wide, and previously unrecognized, range in their boron contents and isotopic compositions reflecting a complex history involving melt depletion and metasomatism by subduction- and plume-derived components, as well as late stage isotopic exchange related to kimberlite emplacements. Micas from ancient lithospheric harzburgite metasomatized by slab-derived fluids suggest extensive B-depletion during subduction, resulting in low-B, isotopically light compositions whereas kimberlite-related metasomatic products and a sample from the 2 Ga Palabora carbonatite have $\delta^{11}B$ values similar to proposed primitive mantle. The results suggest that subduction of oceanic lithosphere plays a limited role in the B geochemistry of the convecting mantle.

DEDICATION

To Gramps, John B. Sweeney III, collector of degrees.

TABLE OF CONTENTS

APPENDIX Page

LIST OF TABLES

LIST OF FIGURES

CHAPTER 1. INTRODUCTION

1.1. Boron and its distribution among various Earth reservoirs

Boron is potentially well suited for tracing the recycling of surface volatiles into the mantle because it is an incompatible, fluid-mobile element. Boron is bound in hydrous fluids as a $B(OH)_3$ species where B is in trigonal coordination and B dissolved in silicates is in tetrahedral coordination. The heavier isotope, ^{11}B, prefers trigonal coordination leading to the large fractionations observed in nature (see "Reviews in Geochemistry," volume 33 for an extensive description of the geochemical behavior of boron). The incompatibility of B implies that its concentration in the mantle is intrinsically low due to the removal by partial melting, and therefore that its later re-enrichment by a variety of processes over time may be easily detected. The utility of boron, in this respect, is augmented by the wide range in boron isotopes and boron concentrations in terrestrial materials (Figure 1 & 2). Seawater (4.5 ppm) and the continental crust (10 ppm) are relatively enriched in boron concentrations with $\delta^{11}B$ values of +39.5‰ and −10.5‰, respectively (Spivack and Edmond, 1987; Chaussidon and Albarède, 1992). The canonical primitive mantle is characterized by boron concentrations of ≤ 0.1 ppm and a boron isotopic composition of −10 ± 2‰ (Chaussidon and Jambon, 1994; Chaussidon and Marty, 1995; Gurenko and Chaussidon, 1995; Roy-Barnman et al., 1998). These estimates for the primitive mantle are based on the measurement of the boron concentrations and isotopic composition of ocean island basalts (Chaussidon and Marty, 1995). Other oceanic basalts, such as MORB, display mostly lower $\delta^{11}B$ values and it has been suggested that hydrothermal alteration or assimilation of crustal components (or sediments) may be responsible for modifying their boron isotopic signatures from values originally similar to those of the primitive mantle (Chaussidon and Marty, 1995). In contrast, subduction-related basalts have higher B concentrations and $\delta^{11}B$ values consistent with the presence in their source of boron lost from the subducting slab as B-bearing minerals break down and release isotopically heavy boron into the source of arc magmas. Continued subduction of these materials results in the eventual 'drying out' of the slab, with successive releases of H_2O fluid containing less and less boron that is isotopically more and

more fractionated (i.e. lighter) boron isotopes. Thus the SCLM can be hypothesized to interact with rising mantle plume material ($\delta^{11}B$ of ~−10‰) or the time-integrated fluid from subducting slabs with $\delta^{11}B$ much lighter (−20 to −40‰) recycled materials affected by seawater-alteration (Moran et al., 1992). Conclusions about the B isotope composition of B-poor mantle reservoirs are rendered somewhat uncertain by the susceptibility of the erupted magmas basalts to contamination by B-rich crustal materials en route to the surface. In contrast, entrained mineral samples from the upper mantle (even when modified during ascent) may show textures allowing such interactions to be detected. Here we report determinations of B concentrations and $\delta^{11}B$ in a suite of mineral samples from the subcontinental lithospheric mantle (SCLM) of southern Africa brought to the surface by fast-erupting kimberlite volcanoes. We examine the potential to characterize the composition and evolution of the SCLM, and the broader implication of these analyses for volatile cycling in the mantle.

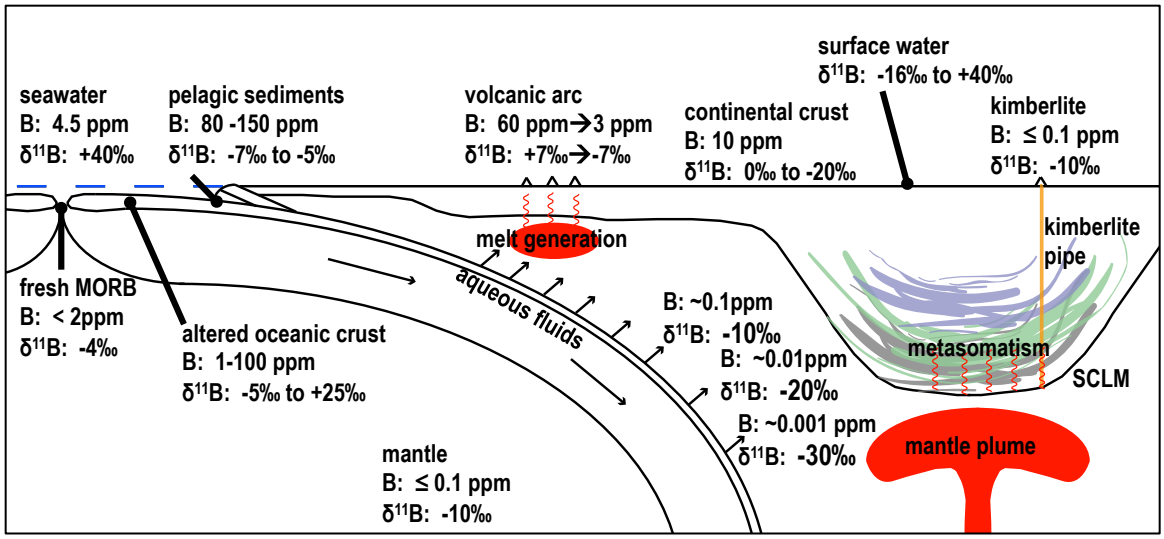

Figure 1. Schematic cross section through a subduction zone and craton with B concentrations and $\delta^{11}B$ values for natural reservoirs (modified from Wunder et al., 2005). Data from the following sources: seawater—Spivack and Edmond (1987); pelagic sediments—Ishikawa and Nakamura (1993); fresh MORB—Leeman and Sisson (1996); altered oceanic crust—Smith et al. (1995); mantle—Chaussidon and Marty (1995), confirmed in this study; volcanic arcs—Rosner et al. (2003); continental crust—Chaussidon and Albarède (1991); kimberlite—this study; surface water—Vengosh et al. (1995). Metasomatism of the subcontinental lithospheric mantle (SCLM) occurs in multiple episodes, with "older" and "younger" events shown by purple, green and gray shading of the SCLM, respectively.

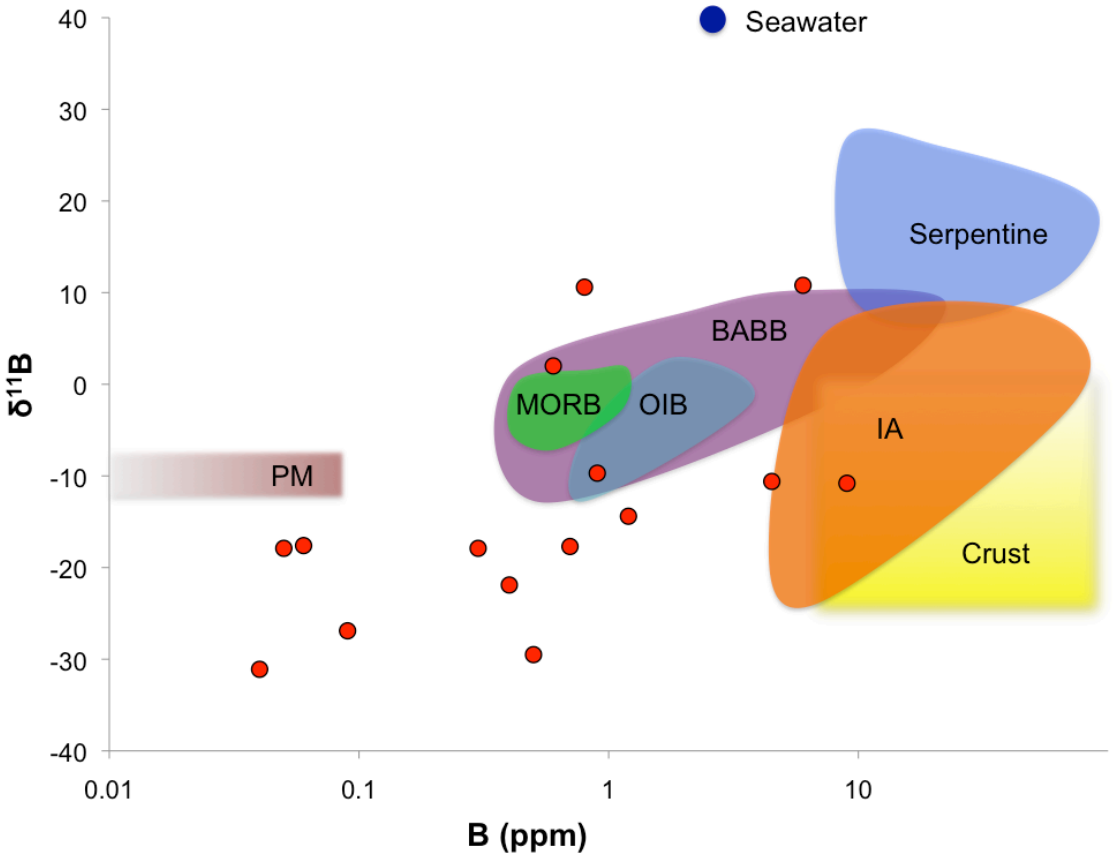

Figure 2: $\delta^{11}B$ vs. B concentrations from major reservoirs. Data from this study plotted as circles—phlogopite data plotted as averages (values recorded in Table I). Primitive Mantle (PM)—Chassidon and Marty (1995); Mid Ocean Ridge Basalts (MORB)—Chaussidon and Jambon (1993); Ocean Island Basalts (OIB)—Chaussidon and Marty (1995), Chaussidon and Jambon (1993); Back arc basin basalt (BABB)—Chassidon and Jambon (1993); Island Arcs (IA)—Rosner et al., (2003), LeVoyer et al., (2008); Crust—Chaussidon and Albarède (1991); Serpentinized peridotites (Serpentine)—Scambelluri and Tonarini (2012). Seawater—Spivack and Edmond (1987).

1.2. Archean subcontinental lithospheric mantle

The subcontinental lithospheric mantle (SCLM) is a geochemical reservoir that is volumetrically 3-4 times larger than the overlying continental crust and thus has the potential to contribute significantly to the global mass balance of some elements. Archean SCLM, which may extend to depths of ~250 km, formed as a buoyant residue of ancient melt-depletion events, for which both subduction- and plume- related melting processes have been proposed (Canil and Lee, 2009; Arndt et al., 2009). This buoyancy, combined with the probable depletion in volatiles and radioactive (heat-producing) elements has resulted in a stable and mechanically rigid lithosphere resistant to destruction by the forces of mantle convection over geologic time. Because it is cold and geologically stable, the SCLM traps upwelling volatile-rich melt and fluids generated in the convecting mantle below, which then react with the melt-depleted lithospheric peridotite to form metasomatic mineral assemblages. The composition of these assemblages conveys information about the origin of their parent fluids, as well as the composition and evolution of the SCLM. Given this model we hypothesized that boron was an element that might represent a record of such processes in the SCLM.

1.2.1. The formation and metasomatism of the Kaapvaal Craton

The Kaapvaal Craton is a region of Archean SCLM that has been the subject of extensive study of both crust and mantle lithosphere. The amalgamation of several smaller cratonic nuclei between 2.5 to 3.0 Ga accompanied by extensive granitoid magmatism and melt-depletion of the underlying mantle lithosphere (de Wit et al., 1992; Carlson et al., 1999; Schmitz et al., 2004, Poujol et al., 2003) resulted in the stabilization of the SCLM. A major phase of subduction-related metasomatism affected the lithosphere during this time (Carlson et al., 1999; Simon et al., 2007). Portions of the craton were impacted by flood basalt magmatism and intrusion of the Bushveld Igneous Complex at 2.65 and 2.05 Ga respectively, with major periods of lithospheric accretion and reworking at the craton margins during the later Kheis and Namaqua orogenies at ~1.6 and ~1.0 Ga (Moen and Armstrong, 2008). The craton was pierced by several episodes of kimberlite magmatism, the major phases being at 200-110 Ma (group II kimberlites) and ~100-75 Ma (group

I kimberlites). The reaction of the kimberlitic precursor magmas and their derivatives with the Kaapvaal SCLM in the Cretaceous resulted in the development of extensive metasomatic assemblages (Erlank et al., 1987; Jones et al., 1982; Kramers et al., 1983; Konzett et al., 1998, 2000; Grégoire et al., 2002, 2003).

The SCLM of the Kaapvaal Craton is sampled via kimberlite-derived xenoliths consisting mainly of Mg-rich garnet harzburgites and lherzolites. The majority of samples are anomalously enriched in orthopyroxene compared to the predicted residua of partial melt extraction at pressures of 3-6 GPa (the pressure of origin) and almost all contain trace phlogopite (Herzberg, 2004; Erlank et al., 1987). This enrichment is believed to reflect the presence of hydrous melts and fluids in an Archean subduction zone setting (Kesson and Ringwood, 1989; Rudnick et al., 1994; Kelemen et al., 1998; Carlson et al., 1999; Bell et al., 2005; Simon et al., 2007). It has been proposed that the Archean lithospheric mantle consisted predominantly of clinopyroxene-free garnet harzburgite with Mg# > 93, and that clinopyroxene and garnet were added by younger silicate melt metasomatism (Simon et al., 2003). In the case of Kaapvaal, much of this may have occurred during the intense thermochemical infiltration and erosion of the cratonic base and margins by plume-derived melts parental to group I kimberlites (Gurney and Harte, 1980; Burgess and Harte, 1999; Bell et al., 2003; Griffin et al., 2003; Kobussen et al., 2009; Janney and Bell, 2010). The infiltration of such magmas into the overlying lithosphere, accompanied by their reactive down-temperature differentiation to carbonatitic residua has given rise to a series of metasomatic assemblages rich in clinopyroxene and phlogopite (Jones et al., 1982; Erlank et al., 1987). The chemical and isotopic composition of these mantle mineral assemblages, and of kimberlite-melilitite-carbonatite magmas erupted at the surface, record the progressive influence of Archean lithosphere on deep-seated magmas that, in the case of group I kimberlites, begin with OIB-like (HIMU-FOZO) geochemical signatures (Kramers et al., 1981, 1983; Smith, 1983; Janney et al., 2002; Nowell et al., 2004; Janney and Bell, 2010; Figure 3). Although a deep lithospheric origin for the HIMU component in mantle derived magmas has been suggested (Hart

and Zindler, 1986; Bell and Tilton, 2001), most studies favor an origin from recycled oceanic crust within the convecting asthenosphere (White and Hoffman, 1982).

In contrast to the metasomatic assemblages related to group I kimberlites that are characterized by the phlogopite-ilmenite-clinopyroxene (PIC) mineral association (Grégoire et al., 2002, 2003), a second lineage of phlogopite-rich assemblages characterized by the presence of potassium-richterite has been linked geochemically to group II kimberlites that originate in enriched (EMII-type) mantle (Dawson and Smith, 1977; Waters, 1987; Sweeney et al., 1993; Ulmer and Sweeney, 2002; Konzett et al., 1998, 2000; Grégoire et al., 2002, 2003). Although both group I and group II kimberlites themselves, were formed by melting that took place within Archean SCLM (Le Roex et al., 2003; Becker and Le Roex, 2006; Becker et al., 2007; Coe et al., 2008), the source of group II kimberlite parental fluids is uncertain—they may have been generated *in situ* within old enriched SCLM (Becker and Le Roex, 2006), from convecting mantle influenced regionally by subduction (as proposed for the Karoo Large Igneous Province by Cox, 1988), or from a plume deriving from an enriched mantle (EM) source (Le Roex, 1986). Whichever of these options applies the EM geochemical signatures of group II kimberlite (i.e., high radiogenic Sr, low radiogenic Nd; Figure 3) suggests ultimate derivation from recycled continental material.

Part of the hypothesis behind our work is that the diversity of metasomatic components identified in previous studies may have boron signatures (concentrations and isotopes) that will allow an investigation of these components and the processes at work at depth through selective analysis of previously characterized samples.

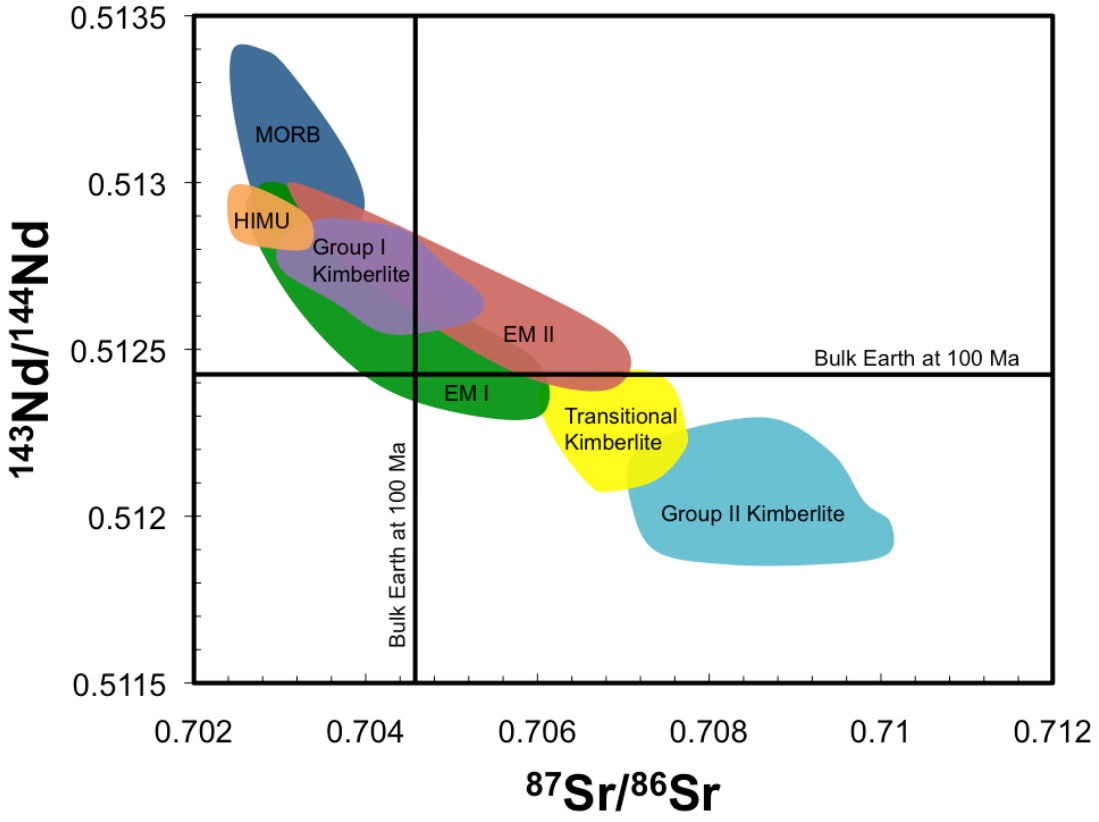

Figure 3: Variation of initial $^{143}Nd/^{144}Nd$ and $^{87}Sr/^{86}Sr$. Colored fields represent published data for South African Group I, Group II and Transitional kimberlites (Smith, 1983; Fraser and Hawkesworth, 1992; Tainton, 1992; Clark, 1994; Nowell et al., 1999, 2004; Coe, 2004; after Becker and le Roex, 2006). MORB, HIMU, EM I and EM II –type basalt fields represent data from Stracke et al. (2003).

CHAPTER 2. METHODS

2.1. Sample Selection

Phlogopite mica, amphibole, and clinopyroxene from mantle xenolith samples collected in southern Africa by J.V. Smith, J.B. Dawson and D.R. Bell were analyzed. Phlogopite is the most widespread phase with relatively high B content in metasomatic assemblages and was therefore targeted for analysis. However, in some cases, phlogopite mica showed inhomogeneous boron and isotopic ratios so coexisting clinopyroxene or amphiboles were also analyzed when possible.

2.1.1. Products of Mesozoic metasomatism

In the case of group I and group II kimberlite magmas, the most primitive components (with respect to minimal lithospheric interaction), are found in subcalcic, Cr-poor clinopyroxene megacrysts (Jones, 1987; Janney and Bell, 2010, 2011). Examples of these are megacrysts ROM270-CI11; ROM273-DI16 (group I) and LAC236, LAC-P (group II). Micas are only encountered in megacryst assemblages precipitated at lower temperatures, typically after substantial magmatic reaction or differentiation (Moore et al., 1992; Bell and Moore, 2004) (MON22; ROM249). These more advanced stages of differentiation and lithospheric reaction are also represented by calcic clinopyroxene megacrysts (Jones, 1987; Moore et al., 1992; Bell and Moore, 2004) (ROM270-DI10) that are sometimes also Cr-rich as a result of their interaction with refractory, melt depleted lithospheric peridotite, in which case they assume an apple green color and are referred to as “Granny Smith” megacryst (Boyd et al., 1984; BFT104). Samples of clinopyroxene and mica megacrysts representing these various stages of group I and group II kimberlite-magma evolution were analyzed (Table II). MARID xenoliths with mineralogical affinities to group II kimberlites but which show radiogenic isotope composition suggesting group I-group II kimberlite mixing were also analyzed (BD3130, BD3655). The above samples are considered to represent mainly fragments of mantle veins representing channel ways of metasomatizing agents. They contrast with the high-temperature garnet lherzolites resulting from metasomatism of the lithospheric base by more primitive magmas in equilibrium with sub-calcic clinopyroxene megacrysts (73-105) and with phlogopite- and clinopyroxene-bearing peridotites

(lherzolites and wehrlites) that represent metasomatites thought to be formed when more differentiated fluids infiltrate surrounding depleted peridotite (BT-7, BD1359). Finally, a sample of mica pyroxenite from the 2.02 Ga Palabora carbonatite complex was analyzed in order to examine the B isotope composition of the mantle in the early Proterozoic.

2.1.2. Products of ancient metasomatism

The age(s) of metasomatism producing dispersed phlogopite and orthopyroxene enrichment in peridotite, as well as occasionally clinopyroxene rich (websteritic) peridotite, is poorly constrained. It is generally accepted that a major fraction of this metasomatism appears to also involve melting that occurred in the Archean, because the Os-isotope model ages of these peridotites are dominated by a peak at ~2.7 Ga (Carlson et al., 1999; Carlson et al., 2005; Pearson and Wittig 2008; Simon et al., 2007). However, Nd and Ar isotope evidence has been presented to suggest that metasomatism may also have occurred in the Mesoproterozoic (Hopp et al., 2008). The geochemical character of this metasomatism is distinct from that resulting from kimberlite metasomatism, being characterized by LILE enrichment and HFSE depletion, with Ba-Ti compositions of micas providing a convenient distinction (Figure 10).

A series of samples was chosen that includes refractory Mg-rich clinopyroxene-free garnet harzburgites (e.g., BFT-153), some of which have sub-calcic garnet compositions indicative of extreme Ca-depletion by partial melt extraction (BFT137; BFT141a; BFT147), as well as pyroxene-rich websteritic compositions (BFT405; BFT297). Orthopyroxene- and phlogopite-rich samples (BFT137, BFT141a) are hypothesized to represent addition of hydrous Si-rich fluids or melts to a harzburgite protolith (Bell et al., 2005), whereas the websteritic samples are suggested to have formed from reaction of a more Ca-rich, perhaps granitoid melt with harzbugite in a mantle wedge setting (Rapp et al., 2010). Sample BFT147 is a relatively orthopyroxene-poor, dunitic garnet harzburgite with accessory chromite and coarse phlogopite that is notably Cl-rich (Bell et al., 2005). This sample has been suggested as a potential example of Archean peridotite protolith showing only incipient orthopyroxene enrichments.

2.2. Sample Descriptions

2.2.1. 73-105, Frank Smith mine

Sample 73-105 is a coarse granular undeformed garnet lherzolite with secondary mica. This sample was a piece of a 1" round thick section (~10 X 5 mm). Garnet makes up a large area of the thin section rimmed by kelyphite and phlogopite. The garnet here is fractured. Olivine and orthopyroxene makes up the remainder of the mineralogy. Serpentinization is pervasive within this sample associated with the olivine. This sample was studied in thin section: Hervig's garnet lherzolite PTS-1 (polished thin section 1). SIMS analyses were performed on the thin section and data was collected for phlogopite, serpentine, garnet and pyroxene.

2.2.2. BT-7, Bultfontein

BT-7 is a coarse grained garnet lherzolite with mica. This sample was a piece of a 1" round thick section, measuring to about 12 X 4 mm. The sample is composed of coarse grains of orthopyroxene. The olivine in this sample, the second most abundant mineral, has been heavily serpentinized. The garnet crystal present in this sample is rimmed by kelyphite. There is one large grain of clinopyroxene (3 mm) in this sample. The pristine tabular phlogopite is seen on the edge of the sample. This sample was previously studied by Delaney et al. (1980) characterizing the mica as "P_K" where the "P" stands for primary mica type and the "K-subscript" indicates that the mica exists in kelyphitic rims around a garnet. The abbreviation, "P_K," is inferred to represent primary textured mica in kelyphitic rims around garnet. This is confusing because it is not explicitly explained in the figure caption and thus could be looked at as a mistake. Although this was classified as primary *textured* mica in Delaney et al. (1980), it is unlikely to be primary in nature because it is found in a reaction rim around garnet. This sample was studied in thin section: Hervig's garnet lherzolite PTS-2 (polished thin section 2). Phlogopite and pyroxene were targeted using SIMS.

2.2.3. BD1359, Matsoku

BD1359 is a coarse granular rutile-garnet lherzolite with evidence of past shearing and metasomatism. This sample is a piece of 1” round thin section measuring to ~10 X 5 mm. The modal mineralogy is difficult to estimate because of the small sample size. This sample is comprised of orthopyroxene, olivine, clinopyroxene, garnet, phlogopite, and rutile (listed in descending abundance). This sample has been heavily sheared. The highly strained olivine neoblasts have annealed and coarsened into a granuloblastic texture. Garnets have been fractured and stung-out. Delaney et al. (1980) reported this sample to have ‘unusual’ primary. The mica in thin section has silicate inclusions. Phlogopite in sample was studied by SIMS: Hervig’s garnet lherzolite PTS-2 (polished thin section 2).

2.2.4. BD3130, Bultfontein

BD3130 is a MARID xenolith. The thin section is 1” round and is a coarse grained rock. Pyroxene is the most abundant mineral in sample. The richterite and phlogopite are concentrated in a vein ≥ 1 cm in width, which spans across the section making up about 25% of the sample. Additional lenticular streaks of this assemblage are seen within the sample. Richterites in this sample are nearly euhedral showing 120/60º cleavage and pleochroism. The micas also show distinct cleavage traces and appear in coarse patches within the vein. The opaque mineral(s), making up about 1% of the modal mineralogy, is likely ilmenite. Rutile is also present in trace amounts in this sample. K-richterite and phlogopite mica were analyzed using SIMS and EMP. This sample was analyzed in thin section: BD3130 (phlogopite and amphibole) (Hervig’s collection).

2.2.5. BD3655, Bultfontein

This sample is a heavily metasomatized olivine-rich peridotite with veins of amphibole-rich material now dominating the rock. Mica and ilmenite make up about 10% of the sample. The Mg-ilmenite is present as elongate crystals. The rock has also been serpentinized. Clinopyroxene is present as an accessory mineral. BD3655 was analyzed by Hervig by SIMS.

The sample was mislaid prior to this study but is thought to be similar to BD3647, documented in Jones et al. (1982).

2.2.6. PB_1, Palabora

PB_1 is a mica pyroxenite from the Palabora carbonatite complex that measures to 15 X 10 X 5 cm. In hand sample, there are large bands of phlogopite the mineralogy (~50%). The clinopyroxene and apatite are similar in appearance and make up about ~35% of the mineralogy. Calcite is also present making up about 5% of the sample. The original hand sample is part of Bell's collection. This sample was studied (by SIMS) in a grain mount made for this work: MGMt-3 (phlogopite and clinopyroxene) (Guild's collection).

2.2.7. ROM-249, Monastery

This Monastery mica megacryst was about 3 X 0.5 X 1 cm. The sample appears almost asbestiform and friable, apparently due to deformation. Individual fragments, broken from the megacryst, were heavily kinked under high magnification. The phlogopite megacryst is part of Bell's collection. This sample was studied (by SIMS and EMP) in a grain mount made for this work: MGMt-1 (phlogopite) (Guild's collection).

2.2.8. BFT153, Bultfontein

BFT153 is a garnet harzburgite xenolith with porphyroclastic texture. In hand sample it appears to be coarse granular but in thin section the olivines have been recrystallized. The exterior of the sample shows evidence of weathering. In thin section, the mineralogy is dominated by olivine (~65%) and orthopyroxene (~20%). The olivine has been heavily fractured and serpentinized. The garnet appears in large clots making up ~10% of the modal mineralogy in thin section. There is a spatial relationship between the garnet and orthopyroxene. Phlogopite is found within the garnet clots, almost exclusively, and makes up ~2% of the mineralogy. Opaque are seen around the olivine. This hand sample is part of Bell's collection. This sample was

studied (by SIMS and EMP) in a grain mount made for this work: MGMt-2 (phlogopite) (Guild's collection).

2.2.9. BFT104, Bultfontein

This clinopyroxene megacryst (measures 6 X 3 X 7 cm) has a rare phlogopite inclusion that measures ~5 X 5 X 1 mm. The clinopyroxene is referred to as a "Granny Smith" because of its bright green color, suggesting a Cr-rich nature. This hand sample and grain separates are part of Bell's collection. This sample was analyzed by SIMS in a grain mount made for the current study: MGMt-3 (phlogopite and clinopyroxene) (Guild's collection).

2.2.10. BFT297, Bultfontein

Sample BFT297 has two distinct coarse granular lithologies: a garnet lherzolite and a garnet websterite with primary mica. The whole sample measures to ~14 X 10 X 6 cm and is ellipsoidal in shape. The sample has a weathering rind that is a few millimeters in thickness. The coarse granular garnet lherzolite section has trace clinopyroxene. The pyroxene-rich part is an orthopyroxene-rich garnet websterite with sparse clinopyroxene and substantial primary phlogopite. This hand sample and grain separates are part of Bell's collection. This sample was studied in a grain mount made for this work: MGMt-2 (phlogopite) and MGMt-4 (garnet) (Guild's collection).

2.2.11. BFT141a, Bultfontein

Sample BFT141a is coarse granular graphite mica bearing garnet harzburgite. The crystals are nearly equigranualr. This sample has nearly equal abundances of olivine and orthopyroxene. Garnets are fairly evenly dispersed among the other grains. Some of the garnets show small kelyphitic rims. The small percentage of opaque mineral is graphite. Phlogopite seems to be spatially related with orthopyroxene. This hand sample and grain separates are part

of Bell's collection. This sample was studied in a grain mount made for this work: MGMt-2 (phlogopite) and MGMt-4 (garnet) (Guild's collection).

2.2.12. BFT405, Bultfontein

Sample BFT405 is a xenolith measures to ~25 X 12 X 13 cm and is approximately ellipsoidal broken along its long axis. The mineralogy along the fractured surface does not seem to be different from the sample as a whole. The exterior of the xenolith has a thin rind of weathered minerals. The bulk of this xenolith is composed dominantly of orthopyroxene (~40%) and olivine (~35%). Phlogopite in this sample is concentrated in veins making up ~10% of the mineralogy. Clinopyroxene crystals are found throughout the sample and are coarse (~5mm crystals on average). Garnets are fairly sparse making up < 5% of the modal mineralogy. BFT405 is a pyroxene-rich garnet lherzolite. This hand sample and grain separates are part of Bell's collection. This sample was studied in a grain mount made for this work: Mt-168 (clinopyroxene and phlogopite) (Bell's collection), MGMt-4 (phlogopite and garnet) (Guild's collection).

2.2.13. BFT404, Bultfontein

Sample BFT404 is a pyroxene-rich garnet lherzolite xenolith that measures to 14 X 11 X 12 cm. This sample is nearly spherical but irregularly shaped with two fractured surfaces. The weathering rind on this sample is 2-5 mm thick and covers the non-fractured surfaces. The bulk of this xenolith is composed nearly equal proportions of orthopyroxene and olivine. Garnets are relatively abundant and evenly dispersed, making up ~15% of the modal mineralogy. Phlogopite in this sample is rare (< 1%). Clinopyroxene crystals are sparsely scattered throughout the sample (~2%) and relatively small (~1mm crystals on average). This hand sample and grain separates are part of Bell's collection. The xenolith was studied in a grain mount made for this work: Mt-168 (clinopyroxene and phlogopite) (Bell's collection), MGMt-4 (phlogopite and garnet) (Guild's collection).

2.2.14. MON22, Monastery

MON22 is a phlogopite megacryst in kimberlite matrix. This phlogopite is about 2 X 0.5 X 0.5 cm and is prism-like in shape. This mica appears undeformed when observed under high magnification. This hand sample is part of Bell's collection. This sample was studied (by SIMS and EMP) in a grain mount made for this work: MGMt-1 (Guild's collection).

2.2.15. BFT137, Bultfontein

Sample BFT137 is a mica garnet harzburgite with a vein of phlogopite-bearing garnet orthopyroxenite. The sample measures to 40 X 22 X 15 cm and has an ellipsoidal shape and is fractured on its long axis. The sample is fractured along the vein and shows a gradation from the phlogopite-bearing garnet orthopyroxenite into a clinopyroxene-free garnet harzburgite with sparsely distributed phlogopite. The boundary between the vein and the host material is indistinct in thin section but obvious in hand sample. The vein is dominated by enstatie with some garnet, subordinate olivine and abundant, coarse phlogopite and large sub-spherical to euhedral sulfide grains (Bell et al., 2005). This sample contains clear petrographic evidence for metasomatism (Bell et al., 2005). This hand sample is part of Bell's collection. This sample was studied (by SIMS and EMP) in a grain mount made for this work: MGMt-2 (phlogopite) and MGMt-4 (garnet) (Guild's collection).

2.2.16. BFT147, Bultfontein

BFT147 was also studied by Bell et al. (2005) and described as uniformly orthopyroxene-poor, olivine-rich garnet harzburgite containing sparse subcalcic garnet and relatively abundant discrete magnesiochromite. The xenolith measures to 20 X 10 X 10 cm. This samples is said to have much less garnet and enstatite than BFT137 (described above). Large patches of coarse phlogopites are present. Magnesiochromite makes up ~2% of the samples. Enstatite observed in this sample has a poikolitic habit, which suggests growth from an intergranular medium. This

hand sample is part of Bell's collection. This sample was studied (by SIMS and EMP) in a grain mount made for this work: MGMt-2 (phlogopite) (Guild's collection).

2.3. Sample Preparation

2.3.1. Sample Mounts

Sample mounts were prepared using mineral separates. Aluminum discs (1" round) with 8 wells were utilized for this study in an effort to minimize the use of epoxy. EpoxiCure™ Epoxy Resin was used for all sample mounts because of its composition. According to studies conducted at Ion Microprobe Facility at University of Edinburgh, EpoxiCure™ Epoxy Resin only contributes 0.3 counts per second of ^{11}B to the average signal (http://www.geos.ed.ac.uk/sidecar/ion-microprobe/epoxy-resins/compositions/).

2.2.2. Orientation of Micas

In an attempt to make a better mica mount I practiced mounting micas in different orientations. Samples were mounted on the basal pinacoid (a axis) and on the 'book end' (b or c axis). When mounted on the 'book end' the grains polished well. Those grains mounted on the basal pinacoid had varying success in polishing. Micas that did not polish well on the basal pinacoid may have been unintentionally placed on an angle. More work is needed to determine if mica orientation has any significant influence on the stability or consistency of analytical measurements.

2.3.3. Mannitol

To reduce boron contamination, I treated all samples with a 1.82% mannitol solution (after Williams et al., 2001). The samples were submerged in the solution and were sonnified for at least an hour. They were left to soak for 15-24 hours. The samples were then removed from the mannitol and sonnified in boron free water for about ten minutes. The samples were then doused with boron free water to remove any mannitol crystals that may have formed over duration of the treatment. The samples were dried in the oven ~150ºC.

After all necessary decontamination steps are taken a gold sputter coat is applied to the surface of the sample using a sputter coater. The sputtered gold coat should be 20-40nm thick (http://sims.ess.ucla.edu/resources/SAMPLEPREP.php).

CHAPTER 3. ANALYTICAL METHODS

3.1. Secondary ion mass spectrometry

3.1.1. Instrumental set up

The concentrations and isotopic compositions of boron in phlogopite, amphibole and coexisting anhydrous assemblages were measured using the Cameca IMS 6f SIMS at Arizona State University. Analyses were performed using a $^{16}O^-$ primary ion beam accelerated to −9.0keV with a beam current of 15-50 nA focused to a 30-50 μm spot. Ion intensities were measured after 5-10 minutes of pre-sputtering in an effort to reach steady-state conditions and reduce the effects of surface contamination. The transfer optics were set to produce an imaged field of ~60 μm with a field aperture of 750 μm diameter was placed on the ion optical axis. $^{11}B^+$ and $^{10}B^+$ were measured for 4 and 16 seconds per cycle, respectively, and integrated over 150-350 cycles depending on boron concentration.

The concentrations of targeted trace elements (Li, F, Ti, Rb, Sr, Zr, Nb, Ba, and Ta) were also determined for selected samples using the Cameca 6f SIMS following conventional energy filtering methods described by Zinner and Crozaz (1986) and Shimizu et al., (1978). We used a $^{16}O^-$ primary ion beam accelerated to −12.5 keV with a beam current of 20nA focused to 20-40 μm diameter spot. Ion intensities were measured after 5 minutes of sputtering to ensure steady state was reached. A mass resolving power of ~300 was used with the same transfer optics as used for the isotope measurements. All trace elements (with the exception of yttrium) were counted for 2 seconds per cycle, while yttrium was measured for 4 seconds per cycle.

The mass resolving power is a measure of the ability to distinguish two peaks of slightly different mass-to-charge ratios in a mass spectrum. The resolution is defined by the ratio of the nominal mass to the actual mass of the targeted species minus the interfering species' actual mass. For the analyses here a MRP of ~1000 was required to resolve $^{10}BH^+$ from $^{11}B^+$ (Figure 3) and $^{30}Si^{3+}$ from $^{10}B^+$. High mass resolution spectra were taken on the IMt-1 standard during the

set up of each analysis session. With such boron concentrations often below 1 ppm it is essential to have the interfering species sufficiently resolved.

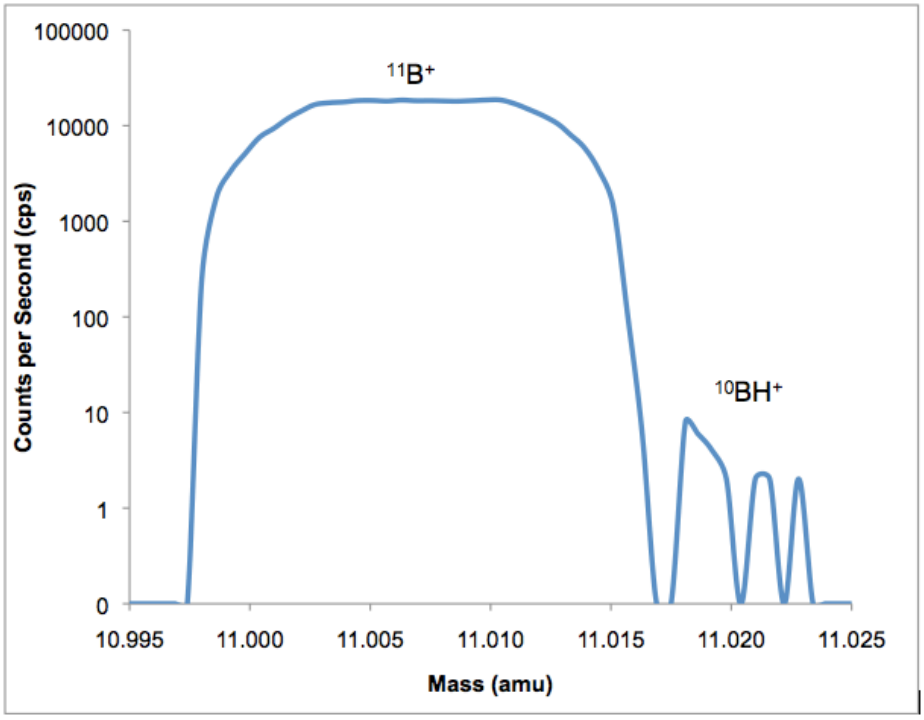

Figure 4: High-resolution mass spectrum of $^{11}B^+$ with atomic mass units displayed on the X-axis and counts per second displayed on the Y-axis. Note $^{11}B^+$ is clearly resolved from the interfering specie $^{10}BH^+$.

3.1.2. Standardization

All samples were standardized to IMt-1 illite clay with 240 ppm of boron and boron isotopic composition of −9‰ (Williams et al., 2001). In earlier measurements of boron isototope standards (IMt-1, synthetic basaltic glass, haplobasaltic glass, and rhyolite glass) at the ASU SIMS lab, no effect of changing sample chemistry on the calibration factor for boron isotope measurements was observed. This is consistent with earlier work by Chaussidon and Marty (1995). However, analysis of NIST 612 glass standard reference material was an exception as a 4‰ change in the isotope calibration was observed compared to the other materials (previously noted by Rosner et al., 2008).

The concentrations of boron were obtained using IMt-1 as a standard. Treating SRM NIST 612 as an unknown returned the bulk analyzed boron concentration within 5%, showing that any matrix effects were small compared to the precision of the analyses of mantle-derived materials.

3.1.3. Analytical Procedures

The standard is used to determine the instrumental mass fractionation. Multiple analyses are done to ensure instrumental stability and proper calibration. Ideally an analysis is done on a flat surface away from the edge that is free of cracks or other obvious imperfections. When moving to the unknown, it is important to be sure charging is compensated prior to executing the analysis. The energy spectrum was used to ensure there was a 40eV window. Charging was manually compensated for throughout an analysis session. This was a major challenge in using this technique because of the high current (30-50nA) being used for most analyses. It was very important to be consistent in checking for charging and manually compensating for it by adjusting the energy window.

In each analysis session, the $^{11}B/^{10}B$ ratio of IMt-1 standard was initially examined in 3-5 points. Comparing the measured ratio to the known value from bulk analyses allowed a calibration factor to be determined. This factor corrects the isotope ratio for the fractionation of the two ions during sputtering, transmission, and detection of the secondary ion signal. This

fractionation is commonly referred to as 'instrumental mass fractionation.' It is expected that the standard will give the same isotope ratio throughout the session, but it is not unusual to see a gradual change in this calibration factor with time, so the standard is run several times during the session.

After calibrating, the unknown materials are analyzed. For both standard and unknowns, it is important to make sure that any charging resulting from the interaction of the negatively charged primary ion beam with the insulating sample is compensated. This is achieved by adjusting the position of the energy window to maximize the secondary ion intensity of the matrix ion (e.g. $^{28}Si^{+}$ or $^{27}Al^{+}$). A consistent instrument set-up was also accomplished by conducting an energy spectrum of standard and unknown to ensure that the range of energy ions (energy window) was set at 40 eV. Carefully checking for sample charging is extremely important to obtaining a reproducible results from session to session.

Once an analysis is executed it is generally it runs for 50-500 cycles (depending on the B count rate) where ^{11}B is counted for 4 seconds and ^{10}B is counted for 16 seconds. Over the course of the analysis the stability is monitored through the comparison of the predicted error (based on Poisson statistics) and the standard error (the cycle to cycle calculated error of the mean) of the $^{11}B/^{10}B$ ratio.

Because of the low boron contents in the phases of interest, the secondary ion signals were low. Ogliore et al. (2011) and Coath et al. (2013) showed that there is an intrinsic bias in the isotope ratio for low signals. Ogliore et al. (2011) in particular found that this bias is reduced to negligible values with the signals for the two isotopes are integrated over the entire analysis and the ratio is calculated from the resulting sums. When compared with the isotope ratio determined by averaging the ratios obtained for each cycle, a bias between the two shows up only when the count rate of $^{11}B^{+}$ declines below 350 counts/s (Figure 5). Because some of the analyses obtained for this study displayed count rates at this level and lower, the integrated ratio was nearly always used.

Ultimately, attempting to obtain good precision on microanalyses of boron-poor phases is limited by how many atoms of boron are consumed during the analysis. In turn, this is limited by how quickly atoms of the micas are removed (a function of the primary beam intensity) and how long we make the analysis (how many cycles of measurement as described above). In fact, many individual measurements have errors in $\delta^{11}B$ that are >5‰. While this is much larger than conventional bulk analyses for boron isotopes (and many other stable isotopes), we can show some advantages of the microbeam approach.

Consider two sets of data from Monastery megacrysts; one of them (MON22) showed large errors in individual analyses, but all of the analyses were within 2σ of the mean, and is labeled as homogeneous. Combining all the analyses into an average and standard error of the mean gives −29.4 ± 0.6‰ (Figure 7). In this case, any of the analyses could be used to represent (with larger precision than the average of 10) the chemistry of this crystal. In contrast, individual analyses of megacryst ROM-249 shows considerable scatter (Figure 7) and the error bars do not overlap. Analyses 2-5 are spatially related (covering an approximate area of 10000 μm^2) but are variable. Analyses 1 & 6 are in separate locations of the same phlogopite crystal. These data cannot be taken to represent one value because they are not within error of each other.

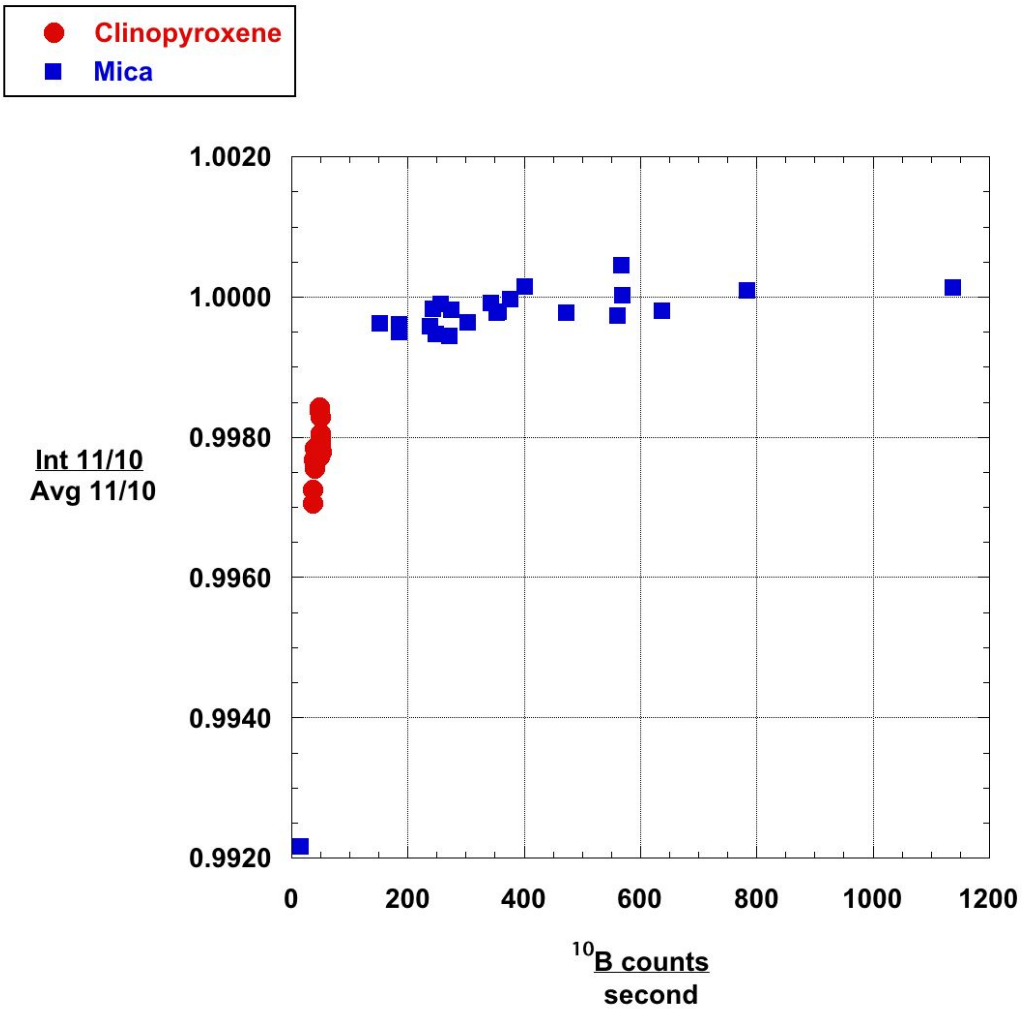

Figure 5: The integrated ratio of $^{11}B/^{10}B$ divided by the average $^{11}B/^{10}B$ plotted against the ^{10}B count rate, where the integrated ratio is the ratio of the summed counts and the average is the average of many (100 or more) individual boron isotopic ratios. Here the difference between these approaches to calculating the average boron isotope ratio is evaluated bases on Ogliore et al. (2011) who found that in some cases averaging a number of ratios leads to an additive bias. This figure shows that below 350 counts/second of ^{10}B the integrated ratio is better representative of the collected data. The lower the B count rate the larger the effect on the ratio. The analyses obtained in this study used the integrated ratio when the boron ion signal was low.

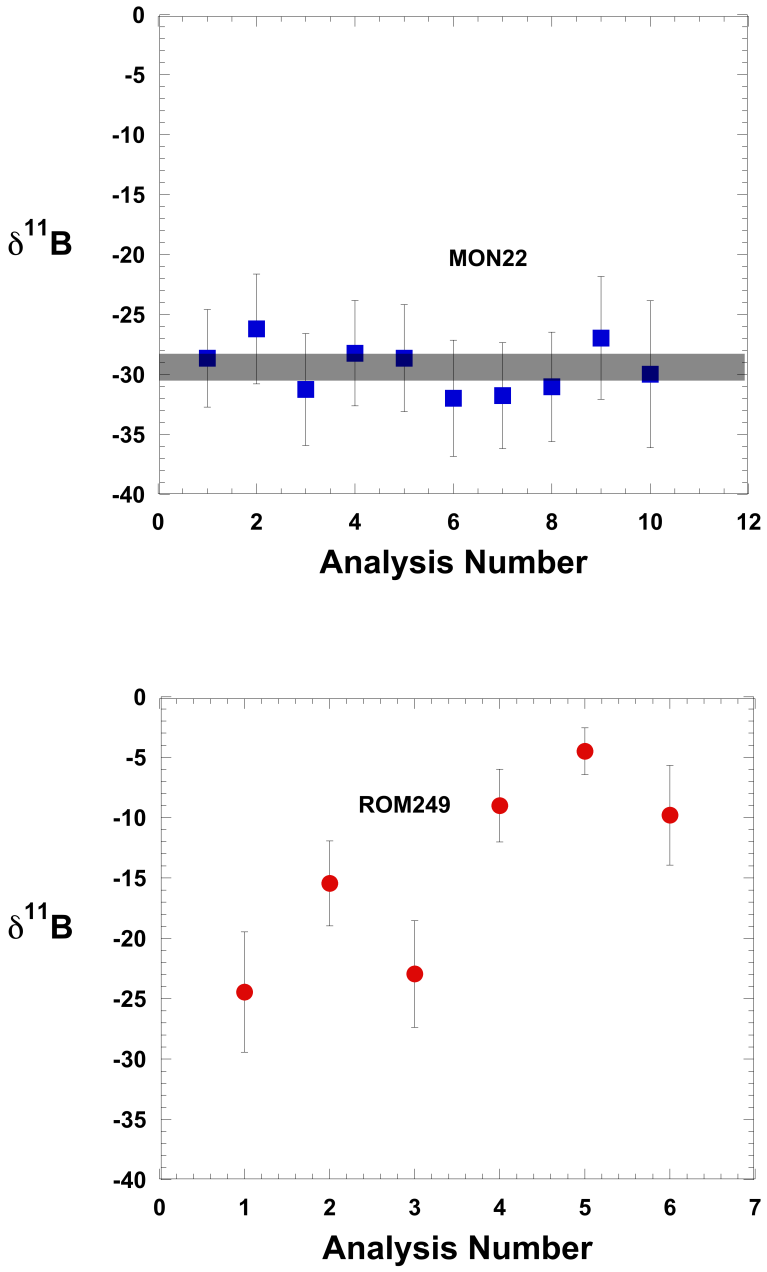

Figure 6: $\delta^{11}B$ vs. Analysis number for two phlogopite megacrysts from Monastery (error bars are 2σ). Results for MON22 and ROM249 are discussed in the text. Gray bar represents the average of MON22 analyses (−29.5 ± 1‰).

CHAPTER 4. RESULTS

4.1. Boron concentrations and isotopic compositions

Boron concentrations and isotopic compositions of phlogopite samples measured in this study are summarized in Table I and Figure 7. Garnet lherzolite phlogopites from Frank Smith, Matsoku and Kimberley display boron contents that range from 0.6 to 6 ppm. The boron isotopic compositions of the phlogopites from garnet lherzolites vary between 2 and 10‰. There appears to be no correlation between the boron content and isotopic composition of these samples. MARID samples have phlogopites with $\delta^{11}B$ around −10‰ and B concentrations ranging from 0.8 to 4.5 ppm. Also falling at −10‰ is the mica pyroxenite sample from Palabora. Despite the similar boron isotopic values, the phlogopite associated with Palabora carbonatite is rich in boron relative to the rest of the sample set (9 ppm). Phlogopite megacrysts from Monastery range from −14 to −30‰ in isotopic composition. One megacryst was heterogeneous with $\delta^{11}B$ values ranging from −5 to −24‰ and B concentrations from 3 ppm to 0.6 ppm (Figure 7). The homogenous Monastery megacrysts had an average $\delta^{11}B$ value around −30‰ and B concentrations of 0.5 ppm. The garnet lherzolite and garnet harzburgite/websterite from Kimberley have similar boron concentrations (0.3-0.4 ppm). The xenolith BFT-297 has a more complex petrologic history as it displays a garnet harzburgite pyroxene-rich section and a more orthopyroxene-rich websteritic section. This sample shows a range of $\delta^{11}B$ values from −2 to −24‰. The garnet lherzolite from Kimberley (BFT-404) has an average boron isotopic composition of −27‰ and a range of concentrations from 0.05 ppm to 0.1ppm. Garnet harzburgites have very light $\delta^{11}B$ values (−18 to −30‰ on average) with low boron concentrations (0.03-0.05 ppm). The olivine-rich garnet harzburgite (BFT147) had the lowest recorded boron concentration in this study (0.003 ppm) and we report no $\delta^{11}B$ value for this mica.

4.2. Trace element data from selected phlogopites

A variety of trace elements were analyzed for a selection of the phlogopite samples and summarized in Table II. Pyrolite-normalized data are shown in Figure 8. All of the studied samples follow the same general pattern with the largest variations over two orders of magnitude for Ti, Ba, and B. The Monastery megacryst (MON22) is notably enriched in Li compared to the other micas.

4.3. Boron isotopic composition of clinopyroxenes

The results of B concentrations and $\delta^{11}B$ measured in clinopyroxene from garnet lherzolites and megacrysts, from Monastery, Palabora, Lace, and Kimberley, are summarized in Table III. On a whole samples range in $\delta^{11}B$ values from −9‰ to −24‰ and concentrations vary from 0.07-0.3 ppm. The two pyroxene-rich garnet lherzolites from Kimberley (BFT404; BFT405) had $\delta^{11}B$ values of −14‰ but with different B concentrations (0.07 ppm and 0.23 ppm, respectively). The sub-calcic megacryst from the group II kimberlite Lace, LAC-236 is relatively light in $\delta^{11}B$ at −17.7‰, with low boron concentration (0.07 ppm). However, the sub-calcic megacryst from Monastery (ROM73_DI16) has a heavier $\delta^{11}B$ value (−11.1 ± 2‰) with a B concentration (0.12 ppm) similar to but slightly higher than the sub-calcic Lace megacrysts (0.12 ppm). The calcic megacryst from Monastery have nearly 0.3 ppm B, which is the highest concentration among this sample set of clinopyroxenes. Based on experiments (e.g. Davis and Boyd, 1966) sub-calcic crystals are presumed to crystallize early while calcic clinopyroxenes represent lower temperatures of formation (more evolved), which is supported by the boron data. The Cr-rich “Granny Smith” clinopyroxene megacryst (BFT104) stands out in this sample set with very light $\delta^{11}B$ (−23.7 ± 4‰).

Table I. Boron abundance and isotopic composition of phlogopite from the subcontinental lithospheric mantle measured by SIMS.

Sample	Source	Rock type	# of analyses	Average $\delta^{11}B$[a]	Average [B][b] ppm
73-105	Frank Smith	Garnet lherzolite with secondary mica	14	10.8±2	6±1
BT-7	Kimberley	Garnet lherzolite with primary mica	4	10.6±2	0.8±0.3
BD 1359	Matsoku	Garnet-rutile lherzolite primary but unusual mica	6	2.0±3	0.6±0.1
BD 3130	Kimberley	MARID	4	−9.7±1	0.8±0.02
BD 3655	Kimberley	MARID	50	−10.6±1	4.5±1
PB_1	Palabora	Mica pyroxenite	4	−10.8±1	9±0.3
ROM-249	Monastery	Mica megacryst	6	−14.4±3	1.2±0.4
BFT153	Kimberley	Garnet harzburgite	1	−17.6±5	0.06±0.01
BFT104	Kimberley	Clinopyroxene megacryst with mica inclusion—Granny Smith	7	−17.7±2	0.7±0.03
BFT297	Kimberley	Two parts: Garnet harzburgite and garnet websterite with primary mica	6	−17.9±4	0.3±0.01
BFT141a	Kimberley	Graphite mica-bearing garnet harzburgite	9	−17.9±2	0.05±0.003
BFT405	Kimberley	Pyroxene-rich garnet lherzolite	10	−21.9±3	0.4±0.02
BFT404	Kimberley	Pyroxene-rich garnet lherzolite	9	−26.9±2	0.09±0.01
MON22	Monastery	Mica megacryst	10	−29.5 ±1	0.5±0.01
BFT137	Kimberley	Mica garnet harzburgite	11	−31.1±2	0.03±0.002
BFT147	Kimberley	Olivine-rich garnet chromite harzburgite	1	----	0.003±0.0006

(a) boron isotopic compositions ($\delta^{11}B$) are reported as the mean value with standard errors based on multiple analyses on phlogopite crystal(s).
(b) boron concentrations calibrated against IMt-1, and synthetic basalt, haplobasalt, and rhyolite glass reported as the mean value with standard errors.

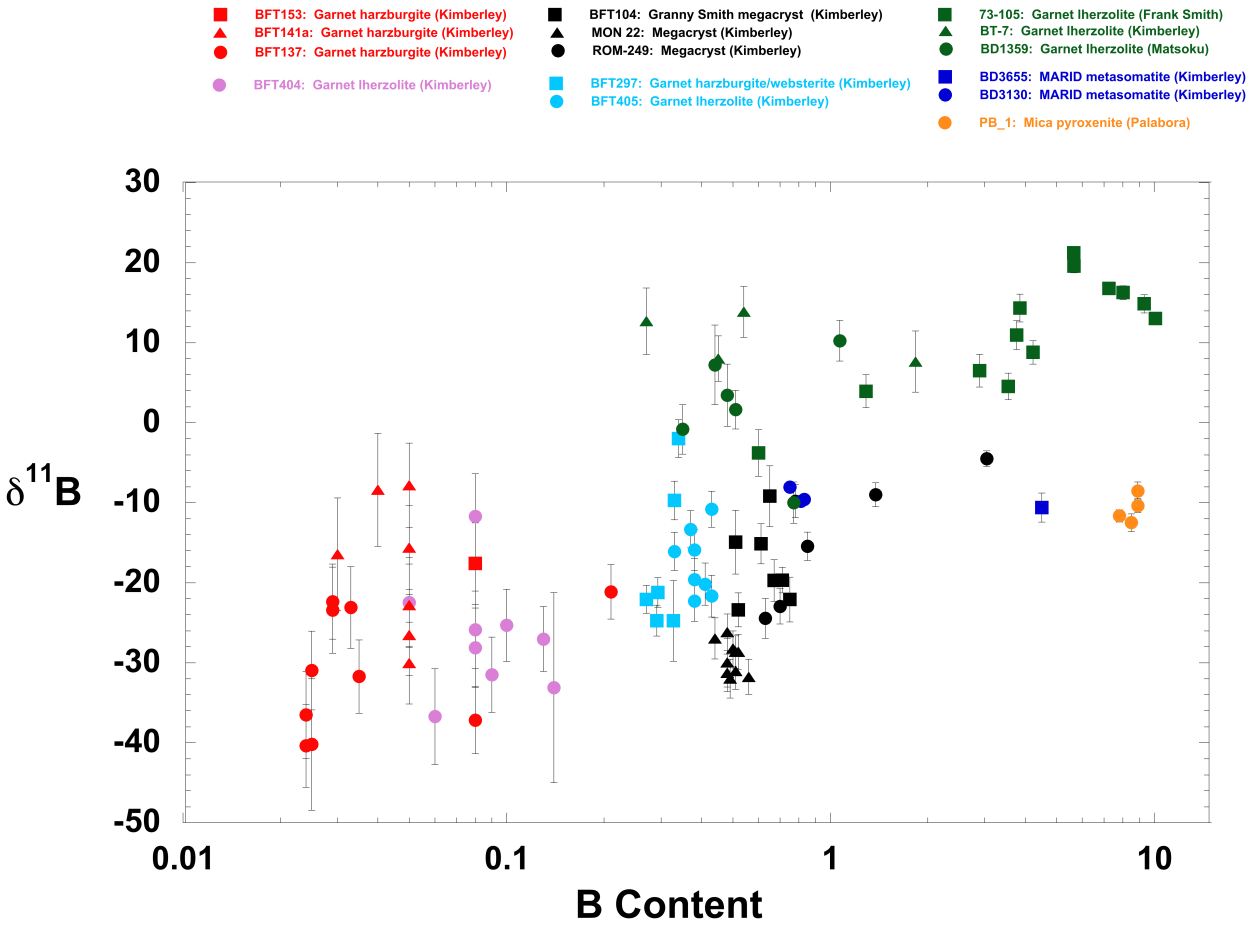

Figure 7: Boron content vs. δ''B values for individual phlogopite analyses (error bar is 1σ). All samples have been grouped according to rock type and geochemistry. Samples plotted in green are interpeted as being influenced by late stage processes in the upper mantle or crust based on petographic evidence. Blue (MARID) and orange (pyroxenite) samples are near 'canonical' mantle values ($\delta^{11}B$: ~-10‰). Light blue symbols represent relatively young metasomatic overprinting based on modes of pyroxene and trace LILE and HFSE abundances. Data plotted in black are megacrysts from the Monastery and Bultfontein kimberlites. Samples plotted in pink are micas from peridotites that have experienced the least Mesozoic metasomatism, but were influenced by metasomatism in the Archean (Bell et al., 2005).

Table II: Trace elements of selected phlogopite samples reported in ppm with 1σ errors. *SiO_2 content estimated.

Sample	SiO_2 (wt%)	Li	F	Ti	Rb	Sr	Y	Zr	Nb	Ba	Hf	Ta	B	$\delta^{11}B$	Mg #
BFT297	41.2	0.96 ±0.01	4150 ±40	7750 ±160	321 ±7	9.5 ±0.1	0.03 ±0.002	4.5 ±0.2	6.2 ±0.2	837 ±13	0.16 ±0.02	0.88 ±0.05	0.3 ±0.01	−17.4 ±3.8	95.6
BFT147	41.8	0.59 ±0.01	2800 ±39	736 ±4	274 ±1	7.1 ±0.3	0.02 ±0.003	7.9 ±0.1	46.1 ±0.3	850 ±8	0.28 ±0.01	2.8 ±0.2	0.003 ±0.0006		96.1
BFT141a	40	0.62 ±0.02	3770 ±330	206 ±0.6	195 ±4	56 ±11	0.03 ±0.003	5.8 ±0.8	27.5 ±0.2	9260 ±485	0.44 ±0.02	1.81 ±0.15	0.05 ±0.003	−17.9 ±2.5	96.4
BFT153	40.0	0.51 ±0.05	1510 ±49	157 ±2	213 ±1	40 ±5	0.025 ±0.003	5.8 ±0.3	18.9 ±0.7	6660 ±525	0.45 ±0.07	1.59 ±0.12	0.06 ±0.01	−17.6 ± 5	96.2
BFT137	41.9	0.53 ±0.04	6670 ±330	564 ±5	235 ±1	6.8 ±0.2	0.016 ±0.004	3.95 ±0.08	12.4 ±0.2	446 ±13	0.08 ±0.02	0.74 ±0.10	0.03 ±0.002	−31.1 ±2.3	96.4
BFT404	~41*	1.56 ±0.13	1640 ±27	1390 ±21	235 ±5	135 ±2	0.111 ±0.003	4.3 ±1.4	15.3 ±0.1	3072 ±26	0.28 ±0.01	1.19 ±0.02	0.09 ±0.01	−21.8 ±3.2	n.a.
BFT405	~41*	1.40 ±0.11	4440 ±89	11300 ±96	377 ±10	10.3 ±0.3	0.047 ±0.009	6.2 ±0.6	19.8 ±0.3	764 ±77	0.19 ±0.04	1.17 ±0.14	0.4 ±0.02	−26.9 ±2.4	n.a.
MON22	41.3	5.5 ±1.1	7890 ±175	7160 ±20	633 ±5	7.6 ±0.8	0.033 ±0.007	7.5 ±0.2	11.9 ±0.2	205 ±1	0.29 ±0.03	0.78 ±0.05	0.5 ±0.01	−29.5 ±0.6	87.9

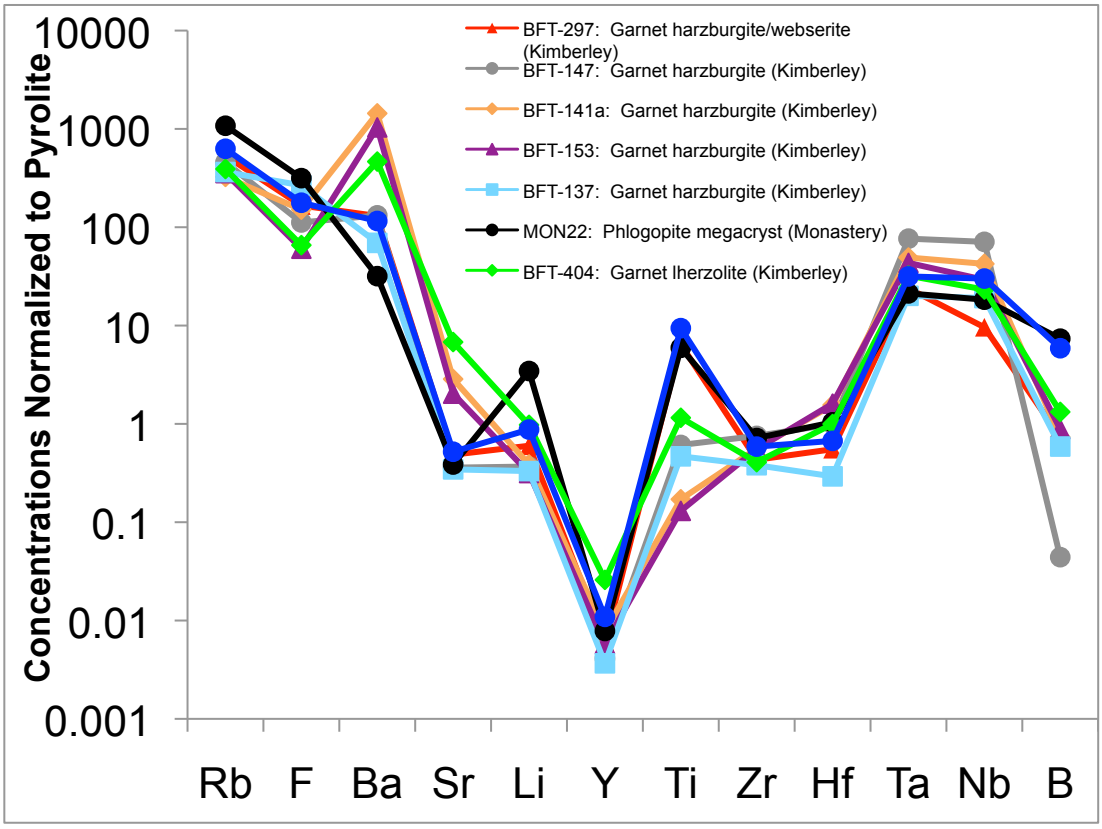

Figure 8. Trace element data from 8 phlogopite samples. The data are normalized to pyrolite values as reported in McDonough and Sun, 1995.

Table III. Clinopyroxene samples measured in this study. Arranged according to $\delta^{11}B$ values. Standard deviation and standard errors are reported for $\delta^{11}B$ and B concentrations, respectively.

Sample	Location	Type	# of analyses	Average $\delta^{11}B$	Average [B] ppm
ROM-270_CI-11	Monastery	Cpx megacrysts coexisting with ilmeninte Sub-Ca	4	-8.9 ± 6 ‰	0.16 ± 0.01
ROM-273_DI-16	Monastery	Sub-calcic megacryst	12	-11.1 ± 6‰	0.12 ± 0.01
ROM-273_DI-10	Monastery	Calcic megacrysts	6	-13.6 ± 3‰	0.28 ± 0.03
BFT-405	Kimberley	Pyroxene rich garnet lherzolite	2	-14.1 ± 6‰	0.23 ± 0.03
BFT-404	Kimberley	Pyroxene rich garnet lherzolite	4	-14.2 ± 10‰	0.07 ± 0.01
PB-1	Palabora	Mica pyroxenite	4	-14.5 ± 2‰	0.9 ± 0.03
LAC-236	Lace	Sub-calcic megacrysts	10	-17.7 ± 5‰	0.07 ± 0.003
BFT-104	Kimberley	Granny Smith Megacryst	4	-23.7 ± 4‰	0.1 ± 0.03

CHAPTER 5. DISCUSSION

5.1. Boron isotope systematics of the Kaapvaal Craton mantle lithosphere

The boron data set can be characterized in terms of three end members: (1) high boron concentrations with heavy and variable isotopic compositions, (2) low intrinsic boron with relatively light isotopic signatures and (3) compositions indistinguishable from estimates of the primitive mantle. Much of the data from this study define a broadly linear trend interpreted here to represent mixing between two or more of these end-members, which we take to represent distinct B-reservoirs. Melt-depletion, re-fertilization, subduction, metasomatism, and near surface alteration have variably affected the samples falling along this trend, and these influences are discussed below.

5.2. “Primitive mantle” B isotope compositions and their significance

The present study shows that several distinct rock types from the SCLM including MARID metasomatites from Bultfontein and mica pyroxenite associated with carbonatite magma from Palabora, and subcalcic clinopyroxene megacrysts from Monastery display similar boron isotopic composition as the primitive mantle ($\delta^{11}B$ ~-10‰) (Figure 9).

It is noteworthy that these comprise some of the most B-rich materical (except those B-rich micas and serpentine obviously affected by late-stage fluid-alteration, as described below). These are therefore samples whose B-isotope compositions appear to be dominated by a convecting mantle component that may have its origin in relatively volatile-rich, poorly degassed mantle. Although geochemical studies of basalts previously suggested that pristine reservoirs of primitive mantle may no longer exist on Earth (Hoffmann, 1988; Hoffmann, 1997), this topic is presently under review (Jackson et al., 2010; Jackson and Jellinek, 2013). Nevertheless, it appears that some lithospheric metasomatites reflect derivation from a source containing juvenile volatiles with primitive-mantle-like $\delta^{11}B$. Furthermore, it appears that the B-isotopic composition of this material has remained unchanged since ~2 Ga, the age of Palabora. The association of

these $\delta^{11}B$ values with kimberlite-related samples implies that group I kimberlite magmas prior to lithospheric interaction are characterized by primitive $\delta^{11}B$ values similar to those of OIB. Isotopic studies of Kaapvaal kimberlites have suggested that these magmas formed by the hybridization with continental lithosphere of melts derived from subducted oceanic crust components within a deep plume source (Janney et al., 2002), similar to models advanced recently for many OIB (Sobolev et al., 2007). Because such subducted crust would be predicted to be highly depleted in B with low $\delta^{11}B$, these results suggest that instead B in kimberlites (and by extension OIB) is dominated by a component derive from the ambient plume matrix material. Thus, it is concluded that subduction of ocean crust does not affect significantly the B budget of the deep mantle, a conclusion reached previously for H as well (Dixon et al., 2002). This is also consistent with the lack of evidence for a secular evolution in the B isotope composition of deep-seated magmas.

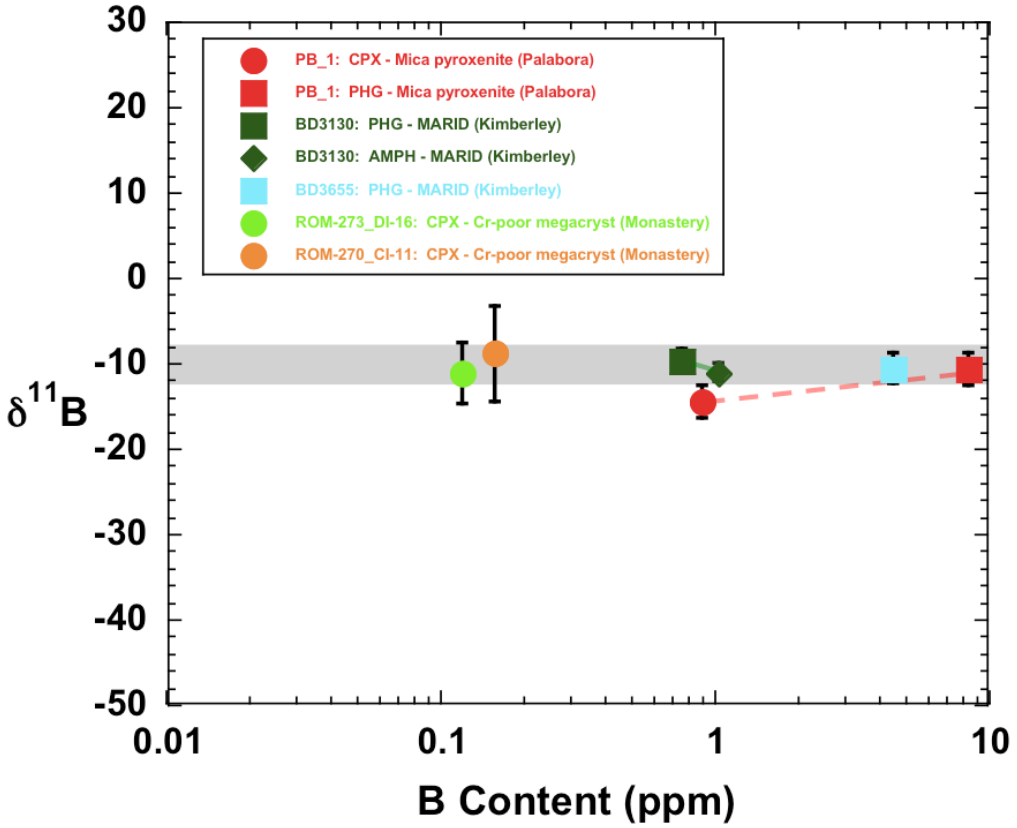

Figure 9: Boron content and isotopic composition of coexisting minerals and megacrysts. Coexisting mineral pairs connected with dashed lines suggest B isotope matrix effects < 5‰. Cr-poor cpx megacrysts from kimberlite, MARID xenoliths, and the mica pyroxenite from the Palabora carbonatite complex all have $\delta^{11}B$ overlapping the canonical mantle value of -10‰. The Granny Smith (Cr-rich) megacryst from Kimberley (not shown) has lower $\delta^{11}B$ reflecting incorporation of B from old metasomatized subcontinental lithospheric harzburgite. Minerals from MARID and carbonatite samples have about an order of magnitude higher B content than kimberlite megacrysts. Shaded region represents mantle value -10 ± 2‰.

5.3. Heavy $\delta^{11}B$ Signatures

Heavy and variable $\delta^{11}B$ values coupled with high boron concentrations are observed in some micas. These micas also display petrographic features indicating a secondary origin. For example, mica in garnet lherzolite 73-105 from Frank Smith displays variable boron (1-15 ppm) and heavy boron isotopes (-3 − +20‰) (see Table I and Figure 7). This sample is also characterized by serpentine veins and kelyphite (see section *2.2.1.* for more details). A garnet-rutile lherzolite (BD1359), from Matsoku, has "primary mica with some unusual features" according to Delaney et al. (1980) but the mica in this rock contains 0.3 to 2 ppm B and $\delta^{11}B$ near 0‰, clearly distinguished from the primitive mantle estimates. The mica in the garnet lherzolite from Bultfontein (BT-7) was labeled as 'primary' based on petrographic textures described by Delaney et al. (1980). However, these micas have B contents that vary from 0.3 to 1.7 ppm and B isotopic compositions between +7.7‰ and +13.9‰. The B isotopic composition of the micas in these samples is, on average, 20‰ heavier than the primitive mantle values.

Along with primary and secondary mica, the peridotites in this study also contain veins of serpentine. In this study we analyzed serpentine from one garnet lherzolite xenolith containing texturally secondary mica (73-105; mica described in the previous section). The serpentine in this sample had $\delta^{11}B$ values ranging from +10‰ to +30‰ and high B concentrations (30-200 ppm). Serpentines and serpentinized rocks are commonly reported to have heavy $\delta^{11}B$ values and variably enriched in boron (Spivack and Edmond, 1987; Chaussidon and Marty, 1995; Scambelluri and Tonarini, 2012; Figure 2). Spivack and Edmond (1987), for example, measured $\delta^{11}B$ and B concentrations of serpentinized peridotites that range from 8.3 to 12.6‰ and 50-81 ppm, respectively. The serpentinization of the peridotites was suggested to occur at low temperatures at shallow depths. These authors concluded that the high B concentrations measured in these altered peridotites is almost entirely secondary as the concentrations of B in pristine peridotites are extremely low (≤0.1ppm) (Spivack and Edmond, 1987). Our results are consistent with these previous observation and interpretations, namely that serpentinizing fluids associated with kimberlite emplacement carry high concentrations of isotopically heavy B. Most

minerals in xenoliths are either inert to the effects of such fluids or display clear evidence of low-temperature reaction assemblages (such as serpentine veins in olivine). Phlogopite undergoes a more subtle form of alteration in which the potassium is leached from the mica structure to form patches of a magnesian phyllosilicate phase within the original phlogopite crystal outline (Luth, 2003). It is possible that isotopic exchange of elements like B and H in micas may occur even before associated chemical effects are evident, with such alteration by fluids plausibly also affecting phlogopite prior to surface emplacement. Late-stage fluids related to kimberlite emplacement, as well as the boron they contain, may have various possible origins, including deuteric fluids derived by exsolution from the magma itself, as well as crustal fluids with varied histories. The heavy $\delta^{11}B$ values that seem to characterize these late-stage alteration products suggest that there is a speciation-dependent isotopic fractionation of B in the parent fluids, similar to that responsible for the overall enrichment of ^{11}B in seawater.

As described in section *3.1.3* (Analytical Procedures), one of the Monastery phlogopite megacrysts was inhomogenous. While the 2 mm crystal displayed textures of shear deformation and kink banding, it was otherwise unremarkable. However, when the $\delta^{11}B$ for these 6 analyses are plotted as a function of the reciprocal boron concentration (Figure 10), we observe a linear correlation most easily explained as a mixing trend between an isotopically heavy, B-rich source (possibly a crustal fluid) and a reservoir with relatively low B concentrations and light boron isotopic values similar to the homogeneous megacrysts (Figure 10). This example shows clearly the potential of late-stage processes to affect the B geochemistry of micas and emphasizes the need to determine both concentrations and $\delta^{11}B$ values from otherwise petrographically pristine grains when seeking original mantle $\delta^{11}B$ and B concentrations.

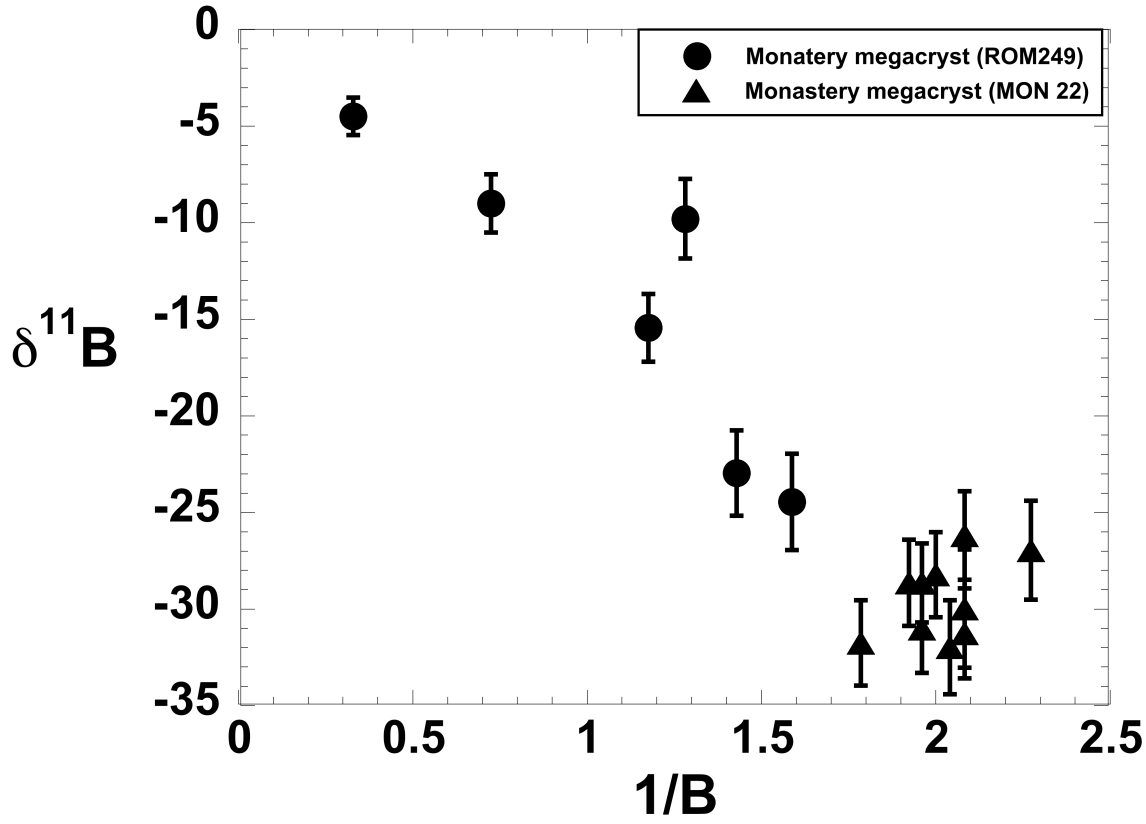

Figure 10. $\delta^{11}B$ vs. 1/B of two Monastery mica megacrysts showing a clear mixing trend between two reservoirs. One megacryst is homogeneous, with low B content and light isotope ratios while another is influenced by a B-rich, isotopically heavy reservoir. Error bars 1σ, isotope measurements re-plotted from Figure 7.

5.4. Light Boron Isotopic Signatures

Micas from seven upper mantle xenoliths displayed lower boron concentrations than the other samples (with some overlap—see Figure 7) and boron isotope ratios much lighter than the canonical primitive mantle value. These include the homogeneous mica megacrysts shown in Figure 10, and the micas in a suite of six peridotite xenoliths interpreted to have been subjected to melt-depletion and metasomatism in the Archean (Bell et al., 2005; Simon et al., 2007). One of these samples (BFT-147) contained too little boron to obtain a precise isotope ratio. The range in $\delta^{11}B$ of this group is -2 − −45‰, with a mean $\delta^{11}B$ of −25‰ (Figure 11). Such isotopically light isotopic signatures cannot simply be explained by temperature dependent fractionation because the fractionation factor of B at T ≥ 600ºC is insignificant and fails to produce a large enough fractionation if one assumes an original isotopic composition similar to that of primitive mantle estimates. It is possible that light boron isotopic values measured in this study record a mixing between an extremely light $\delta^{11}B$ reservoir and a separate reservoir similar to the canonical primitive mantle value, such as group I kimberlite, to produce the values seen here. The lightest $\delta^{11}B$ values recorded in the literature are ~−30‰ in non-marine evaporate and tourmalines (Barth, 1993) and coals with $\delta^{11}B$ as light as −70‰ (Williams et al., 2004). These extremely light values are, however, associated with crustal organic sources and are B-rich relative to the concentrations measured in this study. A mixing model, using this as a reservoir, is unlikely due to generally low mantle B and the lack of organic reservoirs extant at depth. Thus I consider the alternative hypothesis that these signatures are related to subduction processes.

Subducting slabs experience a progressive loss of hydrous fluids with increasing P and T. Due to the favorable bonding environment of ^{11}B in hydrous fluids over silicate melts or minerals, this fluid is isotopically heavy relative to residual solid phases in the slab itself (Wunder et al., 2005; Hervig et al., 2002). This progressive loss of ^{11}B to the departing fluid has been observed in island arc volcanic systems (Rosner et al., 2003; LeVoyer et al., 2008) and exhumed blueschists (Peacock and Hervig, 1999). Supporting this concept is the observation that arc magmas show decreasing $\delta^{11}B$ with increasing distance from the trench. It is therefore predicted

that residual B-bearing minerals in the residual slab have increasingly negative $\delta^{11}B$ values (maybe as light as −20 to −30‰) and lower abundances of boron (Figure 1). The precise nature of the mobile phase responsible for Archean metasomatism is unclear and plausibly includes both siliceous melts and dense hydrous fluids (Rudnick et al., 1994; Ireland et al., 1994; Bell et al., 2005). The probability that Archean slabs routinely underwent melting that metasomatized Archean lithosphere is high (Barth et al., 2001; Rapp et al., 2010). Thus, isotopically light B could be derived from largely dehydrated Archean subducted slabs via melting at depth. Continued dehydration may also be possible, as we do not know when the slab completely degasses. We propose that such ^{11}B-depleted melts and fluids from Archean slabs interacted with the Kaapvaal lithospheric mantle to create the isotopically light orthopyroxene-rich, phlogopite, bearing harzburgites and depleted lherzolites that characterize much of the Kaapvaal craton mantle xenolith suite.

In considering the possibility that fluids evolved from a mostly-dehydrated slab are responsible, we point to sub-calcic garnet harzburgite (BFT147) containing phlogopite with a B concentration of 0.003 ppm as shown in Figure 11. This olivine-rich harzburgite has been interpreted by Bell et al. (2005) as a possible protolith to the more pyroxene-rich metasomatic products generated by Archean subduction-related metasomatism (Kelemen et al., 1998; Simon et al., 2007). These ancient metasomatic products have been variably exposed to later metasomatism by Mesozoic kimberlite-related melts and fluids that add further clinopyroxene and phlogopite, frequently giving rise to isotopic disequilibrium among mineral phases of different generations (e.g., Richardson et al., 1985). However, we have used the geochemical arguments from Bell et al. (2005) to distinguish the samples dominated by a subduction-related component versus those dominated by a kimberlitic component to see if the phlogopites containing significantly lighter boron isotopic values can be similarly correlated. Micas from such garnet harzburgites are represented by the circle, triangle, and diamond symbols in Figure 11. These samples along with one garnet lherzolite, represented by the square symbols, have light boron

isotope ratios (−20 to −30‰) and very low B concentrations (≤0.1ppm) but from 10-100X the B content of the modeled protolith (BFT147).

There is a weak positive correlation between boron content and $\delta^{11}B$ (Figure 11). This can be interpreted as either from an alteration process similar to that shown in Figure 10, or possibly Mesozoic overprinting metasomatism. The large uncertainty in $\delta^{11}B$ measurements when the boron content is so low makes it difficult to distinguish between mixing such as in Figure 10 (which we believe is a relatively shallow phenomenon) and metasomatism in the mantle. However, because mixing of crustal boron (e.g., the high-B, positive $\delta^{11}B$ end member in Figure 10) represents extremely high B contents and heavy isotope ratios, any significant addition of crustal boron to these samples would be easily identified. Thus, phlogopite from samples BFT405 and BFT297 are viewed as samples 'transitional' between a highly depleted component with light $\delta^{11}B$ and low B concentrations the addition of boron with somewhat heavier isotopic ratios (approaching $\delta^{11}B$: −10‰). This transition is more apparent through observing the individual analyses than the average. Figure 11 shows additional chemical differences between metasomatic lineages. The samples we are interpreting as representing subduction related (Archean) metasomatism fall near the y-axis (high Ba/Ti ratios). BFT405 and BFT297 plot along the x-axis with low Ba/Ti ratios characterizing kimberlite-related micas. The connection with subduction relates to a higher solubility of Ba in hydrous fluids than Ti (Spera et al., 2007) thus leading to high Ba/Ti ratios where Ba-rich fluids interact with Ti-poor refractory peridotite to form phlogopite. In contrast, the melts responsible for kimberlites and carbonatites are derived from fertile sources in the convecting mantle that are depleted in fluid-compatible elements (such as boron) and show higher Ti concentrations. However, none of these micas show average $\delta^{11}B$ greater than ~−18‰ (on average), suggesting that there may be some heterogeneity in the boron isotopic composition of different kimberlite magmas.

The extreme depletion of B in ancient subducting slabs, which is indicated by the low B concentrations and very light $\delta^{11}B$ values in Archean metasomatic products, suggests that very little B was returned to the deep mantle by subduction at this time. However, the depleted SCLM

apparently contained even less boron, allowing boron added by subduction related fluids to be detected by analyzing the phlogopites formed during those metasomatic events. The metasomatism from Archean subduction-related fluids has $\delta^{11}B$ values between ~−30 and −20‰, with enrichments in B content (relative to the modeled 0.003 ppm in depleted micas) of 10-100, while still being below 1 ppm. This observation is consistent with that made above on the unchanging $\delta^{11}B$ composition of the convecting mantle with time, and the concentration of mantle B in ambient deep mantle, rather than in its recycled components.

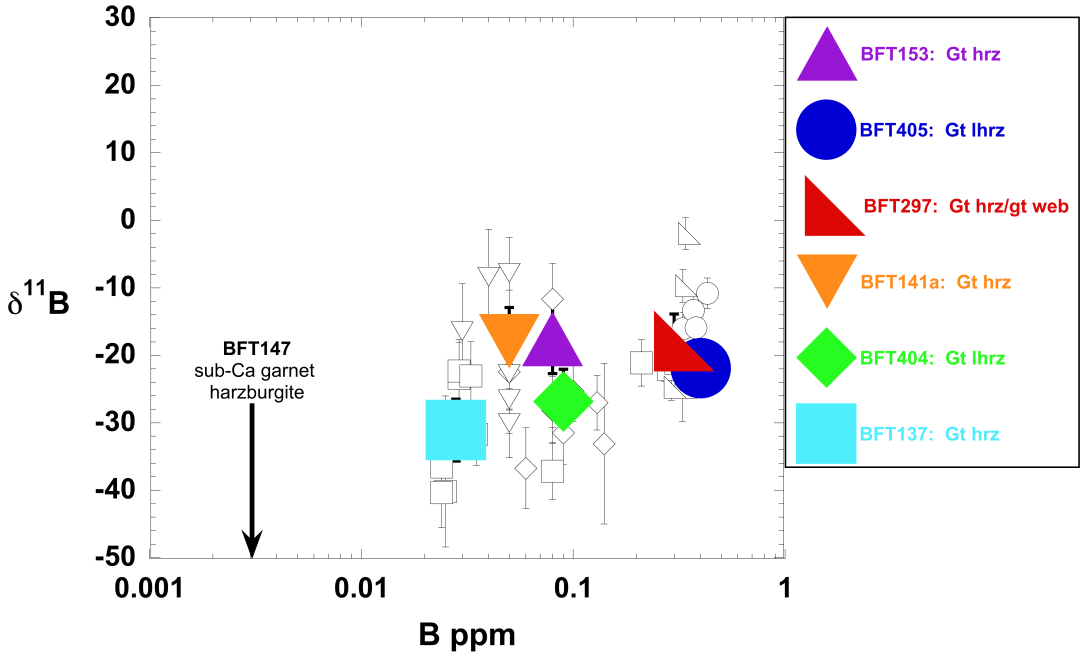

Figure 11. $\delta^{11}B$ plotted against B abundances of phlogopite from Kimberley. Average $\delta^{11}B$ and concentration are plotted in large solid symbols and individual analyses are plotted in open symbols. Garnet harzburgites (gt hrz), garnet lherzolites (gt lhrz), garnet websterite (gt web). Error bars 1σ. Arrow indicates B concentration measured in sub-Ca garnet harzburgite (proposed protolith).

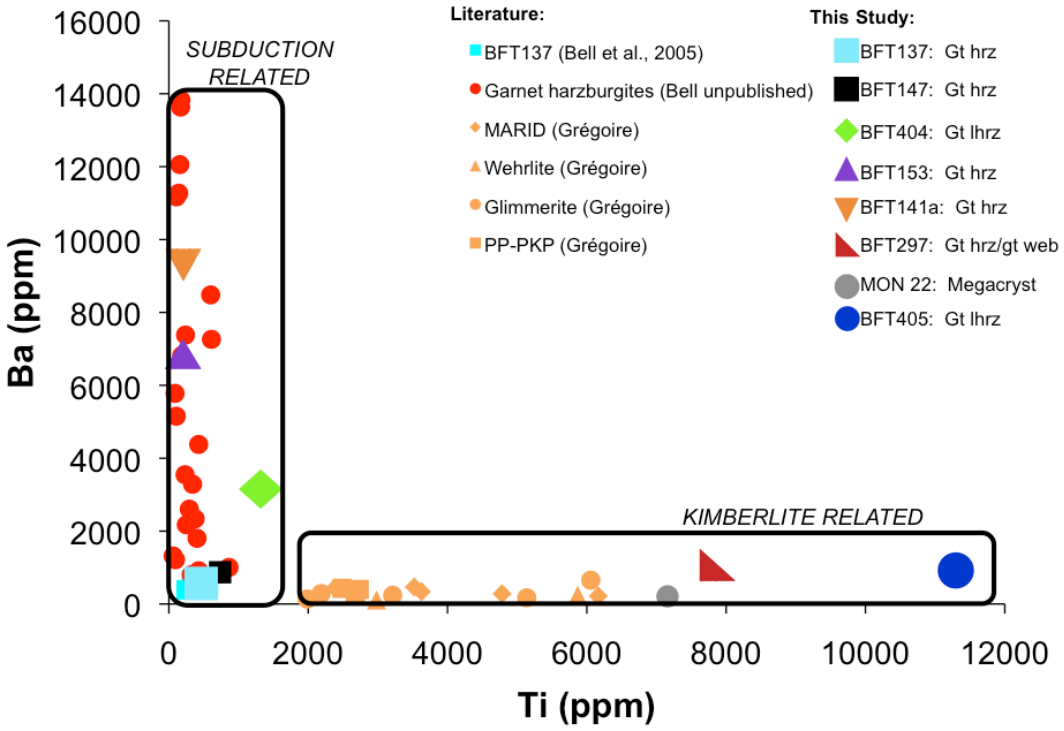

Figure 12: Concentrations of Ba plotted against Ti in phlogopite from Kimberley metasomatic xenoliths illustrating geochemical distinctions among metasomatic lineages. Archean harzburgites plot along the y-axis with high Ba/Ti with subduction related signature. Kimberlite-related metasomatic micas plot with low Ba/Ti along the x-axis. Unpublished data from Gregoire is plotted in the orange symbols. The larger symbols represent samples from this study (BFT-137, BFT-147, BFT-153, BFT-141a, BFT-297, MON22, BFT-404, and BFT-405). Data from Bell et al., 2005 (BFT-137) is represented by blue squares. Unpublished garnet harzburgite data is presented in red squares.

CHAPTER 6. CONCLUSIONS

1. The diversity of the samples derived from the SCLM reflects a complex history of melt depletion and re-enrichment, with mantle phlogopites displaying a wide, previously unrecognized range in B contents and $\delta^{11}B$ for the mantle.
2. Fluid processes during emplacement and/or alteration of the kimberlite have given rise to serpentine and secondary mica in mantle xenoliths with much higher B concentrations and heavier $\delta^{11}B$ values than those of primary mantle minerals.
3. After Archean melt-depletion of SCLM, Archean/Proterozoic metasomatism added trace, but variable, amounts of isotopically light boron (−30‰), relative to primitive mantle (−10‰). This boron was likely derived from extensively dehydrated, B-depleted subducting ocean lithosphere.
4. More recent metasomatism, related to the genesis and eruption of Mesozoic kimberlites, has overprinted subduction-related metasomatism. This overprinting results in higher boron contents and isotope ratios more similar to the canonical primitive mantle.
5. Data from the 2Ga Palabora carbonatite provide no evidence for secular evolution of mantle $\delta^{11}B$ in the convecting mantle.
6. The B isotope geochemistry of metasomatic products in the SCLM supports inferences from the studies of water in oceanic basalts that recycled oceanic lithosphere entering the deep mantle is extensively devolatilized but is recognizable via analyses of trace phlogopite in previously depleted SCLM.

REFERENCES

Arndt, N.T., Coltice, N., Helmstaedt, H., and Grégoire, M., 2009, Origin of Archean subcontinental lithospheric mantle: Some petrological constraints, Lithos, 109: 61-71.

Barrett, D.R. and Berg, G.W., 1975. Complementary petrographic and strontium-isotope studies of South African Kimberlites, Physics and Chemistry of the Earth 9: 619-636.

Barth, S., 1993. Boron isotope variations in nature: a synthesis. Geologische Rundschau 82: 640-651.

Barth, M.G., Rudnick, R.L., Horn, I., McDonough, W.F., Spicuzza, M.J., and Valley, J.W., 2001. Geochemistry of xenolithic eclogites from West Africa; Part I, A link between low MgO eclogites and Archean crust formation. Geochimica Cosmochimica Acta 65: 1499-1527.

Becker, M., and Le Roex, A.P., 2006. Geochemistry of South Africa On- and Off- craton, Group I and Group II Kimberlites: Petrogenesis and Source Region Evolution. Journal of Petrology 47: 673-703.

Becker, M., le Roex, A.P., and Class, C., 2007. Geochemistry and petrogenesis of South African transitional kimberlites located on and off the Kaapvaal craton. South African Journal of Geology 110: 631-646.

Bell, D.R., Schmitz, M.D., and Janney, P.E., 2003. Mesozoic thermal evolution of the southern African mantle lithosphere. Lithos, 71: 273-287.

Bell, D.R., Rossman, G.R., and Moore, R.O., 2004, Abundance and partitioning of OH in a high pressure magmatic system: megacrysts from the Monastery Kimberlite, South Africa. Journal of Petrology, 45: 1539-1564.

Bell, D.R., Grégoire, M., Grove, T.L., Chatterjee, N., Carlson, R.W., Buseck, P.R., 2005, Silica and volatile element metasomatism of Archean mantle: a xenolith-scale example from the Kaapvaal Craton. Contrib Mineral Petrol, 150: 251-267.

Bell, K., and Tilton, G.R., 2001. Nd, Pb and Sr Isotopic Compositions of East African Carbonatites: Evidence for Mantle Mixing and Plume Inhomogeneity. Journal of Petrology 42: 1927-1945.

Burgess, S.R., and Harte, B., 1999. Tracing lithosphere evolution through the analysis of heterogeneous G9/G10 garnets in peridotite xenoliths, I: major element chemistry. In : Gurney J.J., Gurney J.L., Pascoe, M.D., and Richardson, S.H. (eds) *The J.B. Dawson Volume, Proceedings of the 7th International Kimberlite Conference.* Cape Town: Red Roof Design, pp. 66-80.

Canil, D., and Lee, C-T.A., 2009, Were deep cratonic mantle roots hydrated in Archean oceans? Geology, 37: 667-670.

Carlson, R.W., and Bell, D.R., 1997. Re-Os systematics of kimberlite megacrysts inclusions: implications for the source kimberlitic magmas, Extended Abstract, 7th Annual Geochemical Society Goldschmidt Conference, LPI Contribution 921, 43-44, 1997 [abstract].

Carlson, R.W., Pearson, D.G., Boyd, F.R., Shirey, S.B., Irvine, G., Menzies, A.H., Gurney, J.J., 1999. Re-Os systematics of lithospheric peridotites: implications for lithosphere formation and preservation. In: J.J. Gurney, J.L. Gurney, M.D. Pascoe, and S.H. Richardson (eds.), The J.B. Dawson Volume, Proceedings of the 7th International Kimberlite Conference, Red Roof Design, Cape Town, South Africa, 99-108.

Carlson, R.W., Pearson, D.G., James, D.E., 2005. Phsical, chemical and geochronological characteristics of continental mantle. Reviews of Geophysics, 43: RG1001, 1-24.

Chaussidon, M., Albarède, F., 1992, Secular boron isotope variations in the continental crust: an ion microprobe study. Earth and Planetary Science Letters, 108: 229-241.

Chaussidon, M., Jambon, A., 1994, Boron content and isotopic compostition of oceanic basalts: Geochemical and cosmochemical implications. Earth and Planetary Science Letters, 121: 277-291.

Chassidon, M., Marty, B., 1995, Primitive boron isotope compositions of the mantle. Science, 269: 383-386.

Clark, T.C., 1994. An integrated geochemical and isotopic study of the Prieska Province kimberlites from the Republic of South Africa. M.Sc. thesis, University of the Witwatersrand.

Coath, C.D., Steele, R.C.J, and Lunnon, W.F., 2013. Statistical bias in isotope ratios. J. Anal. At. Spectrom., 28,52.

Coe, N., 2004. Petrogenesis of the Swartruggens and Star Group II kimberlite dyke swarms, South Africa. M.Sc., University of Cape Town, 146 pp.

Coe, N., le Roex, A.P., Gurney, J.J., Pearson, G., and Nowell, G., 2008. Petrogenesis of the Swartruggens and Star Group II kimberlite dyke swarms, South Africa: constraints from whole rock geochemistry. Contributions to Mineralogy and Petrology 156: 627-652.

Cox, K.G., 1988. The Karoo Province. In: J.D. MacDougall (Ed.), Continental Flood Basalts. Kluwer, 239-271.

Davis, B.T.C., and Boyd, F.R.,1966. The join Mg2Si2O6—CaMgSi2O6 at 30 kilobars and its application to pyroxenes from kimberlites. Journal of Geophysical Research 71: 3567-3576.

Dawson, J.B., and Smith J.V., 1977. The MARID (mica-amphibole-ruitle-ilmenite-diopside) suite of xenoliths in kimberlite. Geochimica Cosmochimica Acta, 41: 309-323.

de Wit, M.J., Roering, C., and Hart, R.J., 1992, Formation of an Archean continent, Nature, 357: 553-562.

Delaney, J.S., Smith, J.V., Carswell, D.A., and Dawson, J.B., 1980, Chemistry of micas from kimberlites and xenoliths—II. Primary- and secondary-textured micas from peridotite xenoliths. Geochimica et Cosmochimica Acta 44: 857-872.

Dixon, J.E., Leisst, L., Langmuir, C., and Schilling, J-G., 2002. Recycled dehydrated lithosphere observed in plume-influenced mid-ocean-ridge basalt. Nature 420: 385-389.

Erlank, A.J., Waters, F.G., Hawkesworth, C.J., Haggerty, S.E., Allsopp, H.L., Rickard, R.S., and Menzies, M., 1987. Evidence for mantle metasomatism in peridotite nodules from the Kimberley pipes, South Africa. In: Menzies, M., and Hawkesworth, C.J. (eds) Mantle Metasomatism. London: Academic Press, 221-309.

Fraser, K.J., and Hawkesworth, C.J., 1992. The petrogenesis of group 2 ultrapotassic kimberlite from Finsch mine, South Africa. Lithos 28: 327-345.

Grégoire, M., Bell, D.R., Le Roex, A.P., 2002a. Trace element geochemistry of phlogopite-rich mafic xenoliths: their classification and their relationshipto phlogopite bearing peridotites and kimberlites revisited. Contributions to Mineralogy and Petrology, 142: 603-625.

Grégoire, M., Bell, D.R., Le Roex, A.P., 2003. Garnet lherzolites from the Kaapvaal Craton (South Africa): trace element evidence for a metasomatic history. Journal of Petrology 44(4): 629-657.

Griffin, W.L., O'Reilly, S.Y., Abe, N., Aulbach, S., Davies, R.M., Pearson, N.J., Doyle, B.J., and Kivi, K., 2003. The origin and evolution of Archean lithospheric mantle. Precambrian Research 127: 19-41.

Gurenko, A.A., and Chaussidon, M., 1995. Enriched and depeleted primitive melts included in olivine from Icelandic tholeiites: Origin by continuous melting of a single mantle column, Geochimica Cosmochimica Acta 59: 2905-2917.

Gurney, J.J., and Harte, B, 1980. Chemical variations in upper mantle nodules from southern African kimberlites. Philosophical Transactions of the Royal Society of London, A297: 273-293.

Hart, S.R., and Zindler, A., 1986. In search of a bulk-earth composition. Chemical Geology 57: 247-267.

Hervig, R.L., Moore, G.M., Williams, L.B., Peacock, S.M., Holloway, J.R., Roggensack, K.R., 2002. Isotopic and elemental partitioning of boron between hydrous fluid and silicate melt. American Mineralogist Letters, 87: 769-774.

Herzberg, C., 2004, Geodynamic Information in Peridotite Petrology. 45: 2507-2530.

Hoffmann, A.W. 1988. Chemical differentiation of the Earth: the relationship between mantle, continental crust, and oceanic crust. Earth planet. Sci. Lett. 90, 297-314.

Hoffmann, A.W. 1997. Mantle geochemistry: the message from oceanic volcanism. Nature 385, 219-229.

Hopp, J., M. Trieloff, G.P. Brey, A.B.Woodland, N.S.C. Simon, J.R. Wijbrans, Siebel, E. Reitter 2008. 40Ar/39Ar-ages of phlogopite in mantle xenoliths from South African kimberlites: Evidence for metasomatic mantle impregnation during the Kibaran orogenic cycle. LIthos 106, 351-364.

Ireland, T.R., Rudnick, R.L., and Spetsius, Z., 1994. Trace element in diamond inclusions from eclogites reveal link to Archean granites. Earth and Planetary Science Letters 128: 199-213.

Ishikawa, T., Nakamura, E., 1993, Boron isotope systematics of marine sediments, Earth and Planetary Science Letters. 117: 567-580.

Jackson, M.G., Carlson, R., Kurz, M.D., Kempton, P.D., Francis, J., and Blusztajn, J., 2010. Evidence for the survival of the oldest terrestrial mantle reservoir. Nature 466: 853-856.

Jackson, M.G., and Jellinek, A.M., 2013. Major and trace element composition of the high 3He/4He ("FOZO") mantle: Implications for the composition of the bulk silicate Earth. Geochemistry, Geophysics, Geosystems, 14: 2954–2976.

Janney, P.E., Le Roex, A.P., Carlson, R.W., and Viljoen, K.S., 2002. A Chemical and Multi-Isotope Study of the Western Cape Olivine Melilitite Province, South Africa: Implications for the Sources of Kimberlites and the Origin of the HIMU Signature in Africa. Journal of Petrology, 43: 2339-2370.

Janney, P. E. and Bell, D. R. 2011. Pb-Sr-Nd-Hf isotope variations of megacrysts from Mesozoic southern African kimberlites reflect mixing of HIMU melts with deep lithosphere. Goldschmidt 2011 Meeting, Prague Abstr.

Janney, P. E. and Bell, D.R., 2010. Pb isotopic evidence for a cognate origin of Cr-poor megacrsysts in southern African kimberlites. Goldschmidt Conference, 75, p. A458. Geochimica et Cosmochimica Acta, Knoxville, TN.

Jones, A.P., Smith, J.V., and Dawson, J.B., 1982. Mantle Metasomatism in 14 Veined Peridotites from Bultfontein Mine, South Africa. Journal of Geology 90: 435-453.

Jones, R.A., 1987. Strontium and neodymium isotopic and rare-earth element evidence for the genesis of megacrysts in kimberlites of southern Africa. In: P.H. Nixon (ed.), Mantle xenoliths. John Wiley and Sons, Chichester, U.K., 711-724.

Kelemen, P.B., Hart, S., and Bernstein, S., 1998, Silica enrichment in the continental upper mantle via melt rock reaction, Earth and Planetary Science Letters, 164: 387-406.

Kesson, S.E., and Ringwood, A.E., 1989, Slab-mantle interactions 2: the formation of diamonds, Chemical Geology, 78: 97-118.

Kobussen, A.F., Griffin, W.L., and O'Reilly, S.Y., 2009. Cretaceous thermo-chemical modification of the Kaapvaal cratonic lithosphere, South Africa. Lithos 112S: 886-895.

Konzett, J., Armstrong, R.A., Sweeney, R.J., and Compston, W., 1998. The timing of MARID metasomatism in the Kaapvaal mantle: an ion microprobe study of zircons from MARID xenoliths. Earth and Planetary Science Letters, 160: 133-145.

Konzett, J., Armstrong, R.A., Gunther, D., 2000. Modal metasomatism in the Kaapvaal craton lithosphere: constraints on timing and genesis from U-Pb sircon dating of metasomatized peridotites and MARID-type xeonoliths. Contributions to Mineralogy and Petrology 139: 704-719.

Kramers, J.D., 1977. Lead and strontium isotopes in Cretaceous kimberlites and mantle-derived xenoliths from Southern Africa. Earth planet. Sci. lett. 34, 419-431.

Kramers, J.D., Smith, C.B., Lock, N.P., Harmon, R.S., and Boyd, F.R., 1981. Can Kimberlites be generated from an ordinary mantle? Nature 291: 53-56.

Kramers, J.D., Roddick, J.C.M., and Dawson, J.B., 1983. Trace element and isotopic studies on veined, metasomatic 'MARID' xenoliths from Bultfontein, South Africa. Earth and Planetary Science Letters. 65: 90-106.

Leeman, W.P., Sission V.B., 1996, Geochemistry of boron and its implications for crustal and mantle processes. In: Grew, E.S., Anvoitz, L.M. (Eds.), Boron: Mineralogy, Petrology and Geochemistry, Reviews in Mineralogy, vol. 33, pp. 644-707.

le Roex, A.P., 1986. Geochemical correlation between African kimberlites and South Atlantic hotsopts. Nature 324: 243-246.

le Roex, A.P., Bell, D.R., and Davis, P., 2003. Petrogenesis of Group I kimberlites from Kimberley, South Africa: evidence from bulk rock geochemistry. Journal of Petrology 44: 2261-2286.

LeVoyer, M., Rose-Koga, E.F., Laubier, M., Schiano, P., 2008, Petrogenesis of arc lavas from the Rucu Pichincha and Pan de Azucar volcanoes (Ecuadorian arc): Major, trace element, and boron isotope evidences from olivine-hosted melt inclusions. Geochemistry, Geophysics, Geosystems, 9: 1-27.

Luth, R. W., 2003. Mantle volatiles -- distribution and consequences. In The Mantle and Core (ed. R. W. Carlson) Volume 2 Treatise on Geochemistry (editors H. D. Holland and K. K. Turekian), Elsevier-Pergamon, Oxford, 319-361.

Mitchell, R.H., and Crocket, J.H., 1971. The isotopic composition of Strontium in some South African kimberlites. Contrib. Miner. Petrol. 30: 277-290.

Moen, H and Armstrong, R, 2008. New age constraints on the tectonogenesis of the Kheis Subprovince and the evolution of the eastern Namaqua Province, South African Journal of Geology 111: 79-88.

Moore, R.O., Griffin, W.L., Gurney, J.J., Ryan, C.G., Cousens, D.R., Sie, S.H., and Sutter, G.F., 1992, Trace element geochemistry of ilmenite megacrysts from the Monastery kimberlite, South Africa. Lithos, 29: 1-18.

Moran, A.E., Sisson, V.B., and Leeman, W.P., 1992. Boron depletion during progressive metamorphism: Implications for subduction processes. Earth and Planetary Science Letters 111: 331-349.

Nowell, G.M., Pearson, D.G., Kempton, P.D., Noble, S.R., and Smith, C.B., 1999. Origins of kimberlites: a hafnium perspective. In: Gurney, J.J., Gurney, J.L., Pascoe, M.D., and Richardson, S.H., (eds) Proceedings of the VIIth International Kimberlite Conference. Cape Town: Red Roof Design, 616-624.

Nowell, G.M., Pearson, D.G., Bell, D.R., Carlson, R.W., Smith, C.B., Kempton, P.D., and Noble, S.R., 2004. Hf Isotope Systematics of Kimberlites and their Megacrysts: New Constraints on their Source Regions. Journal of Petrology 45: 1583-1612.

Ogliore, R.C., Huss, G.R., Nagashima, K., 2011, Ratio estimation in SIMS analysis, Nuclear Instruments and Methods in Physics Research B, 269: 1910-1918.

Peacock, S.M., Hervig, R.L., 1998, Boron isotopic compositon of subduction-zone metamorphic rocks, Chemical Geology, 160: 281-290.

Pearson, D.G., and Wittig, N., 2008, Formation of Archaean continental lithosphere and its diamonds: the root of the problem, journal of the Geological Society, 165: 895-914.

Poujol, M., Robb, L.J., Annhaeusser, C.J., Gericke, B. 2003. A review of the geochronological constraints on the evolution of the Kaapvaal Craton, South Africa. Precambrian Res. 127, 181-213.

Rapp, R.P., Norman, M.D., Laporte, D., Yaxley, G.M., Martin, H., and Foley, S.F., 2010. Chemical Evoltion of the Chemical Evolution of the Cratonic Lithosphere: Melt—Rock Reaction Experiments at 3-4 GPa and Petrogenesis of Archean Mg-Diorites (Sanukitoids). Journal of Petrology 51: 1237-1266.

Richardson, S. H., Erlank, A. J. & Hart, S. R. 1985. Kimberlite-borne garnet peridotite xenoliths from old enriched subcontinental lithosphere. Earth planet. Sci. Lett. 75, 116-128.

Rosner, M., Erzinger, J., Franz, G., Trumbull, R.B., 2003, Slab derived boron isotope signatures in arc volcanic rocks from the Central Andes and evidence for boron isotope fractionation during progressive slab dehydration. Geochemistry, Geophysics, Geosystems, 4: 1-25.

Rosner, M., Wiedenbeck, M., Ludwig, T., 2008, Composition-Induced Variations in SIMS Instrumental Mass Fractionation during Boron Isotope Ratio Measurements of Silicate Glasses, Geostandards and Geoanalytical Research, 32: 27-38.

Roy-Barnman, M., Wassemburg, G.J., Papanastassiou, D.A., Chaussidon, M., 1998, Osmium isotope compositions and Re-Os concentrations in sulfide globules from basaltic glasses. Earth and Planetary Science Letters, 154: 331-347.

Rudnick, R.L., McDonough, W.F., Orpin, A., 1994. Northern Tanzanian peridotite xenoliths: a comparison with Kaapvaal peridotites and inferences on metasomatic interactions. In: Meyer H.O.A., Leonardos, O. (Eds.), Kimberlites, Related Rocks and Mantle Xenoliths. Proceedings Fifth International Kimberlite Conference, vol. 1. CPRM, Brasilia, pp. 336-353.

Scambelluri, M., Tonarini, M., 2012, Boron isotope evidence for shallow fluid transfer across subduction zones by serpentinized mantle. Geology, 40: 907-910.

Schmitz, M.D., Bowring S.A., de Wit, M.J., and Gartz, V., 2004. Subduction and terrane collision stabilized the western Kaapvaal craton tectosphere 2.9 billion years ago. Earth and Planetary Science Letters 222: 363-376.

Shimizu, N., Semet, M.P., and Allègre, C.J., 1978. Geochemical applications of quantitative ion-microprobe analysis. Geochimica et Cosmochimica Acta 42: 1321-1334.

Simon, N.S.C.,Irvine, G.J., Davies, G.R., Pearson, D.G., and Carlson, R.A., 2003. The origin of garnet and clinopyroxene in 'depleted' Kaapvaal peridotites. Lithos, 71: 289-322.

Simon, N.S.C., Carlson, R.W., Pearson, D.G., Davies, G.R., 2007, The origin and evolution of the Kaapvaal Cratonic lithospheric mantle. Journal of Petrology, 48: 589-625.

Smith, H.J., Spivack, A.J., Staudigel, H., Hart, S.R., 1995, The boron isotopic composition of altered oceanic crust. Chemical Geology: 119-135.

Sobolev, A.V., Hofmann, A.W., Kuzmin, D.V., Yaxley, G.M., Arndt, N.T., Chung, S-L., Danyushevsky, L.V., Elliott, T., Frey, F.A., Garcia, M.O., Gurenko, A.A., Kamenetsky, V.S., Kerr, A.C., Krivolutskaya, N.A., Matvienkov, V.V., Nikogosian, I.K., Rocholl, A., Sigurdsson, I.A., Sushchevskaya, N.M., and Teklay, M., 2007. The Amount of Recycled Crust in Sources of Mantle-Derived Melts. Science 316: 412-417.

Spera, F.J., Bohrson, W., Till, C.B., Ghiorso, M.S., 2007, Partitioning of trace elements among coexisting crystals, melt, and supercritical fluid during isobaric crystallization and melting, American Mineralogist, 92: 1881-1898.

Spivack, A.J., Edmond, J.M., 1987, Boron isotope exchange between seawater and the oceanic crust. Geochimica et Cosmochimica Acta, 51: 1033-1043.

Stracke, A., Bizimis, M., and Salters, V.J.M, 2003. Recycling oceanic crust: Quantitative constraints. Geochemistry Geophysics Geosystems, doi:10.1029/2001GC000223

Sweeney, R.J., Thompson, A.B. and Ulmer, P. (1993) Phase relations of a natural MARID composition and implications for MARID genesis, lithospheric melting and mantle metasomatism. Contrib. Mineral. Petrol. 115: 225-241.

Tainton, K.M., 1992. The petrogenesis of group-2 kimberlites and lamproites from the Northern Cape Province, South Africa. Ph.D. thesis, Cambridge.

Tonarini, S., Pannisi, M., Leeman, W., 1997, Precise boron isotopic analysis of complex silicate (rock) samples using alkali carbonate fusion and ion-exchange separation. Chemical Geology, 142: 129-137.

Ulmer, P. and Sweeney, R. J. 2002. Generation and differentiation of group II kimberlites: constraints from a high-pressure experimental study to 10 GPa . Geochim. Cosmochim. Acta 66, 2139-2153.

Vengosh, A., Heumann, K.G., Juraske, S., Kasher, R., 1994, Boron Isotope Application for Tracing Sources of Contamination in Groundwater. Environmental Science and Technology, 28: 1968-1974.

Waters, F.G., 1987. A suggested origin of MARID xenoliths in kimberlites by high pressure crystallization of an ultrapotassic rock such as lamproite. Contributions to Mineralogy and Petrology, 95: 523-533.

White, W.M. and Hofmann, A.W., 1982. Sr and Nd isotope geochemistry of oceanic basalts and mantle evolution. Nature 296: 821-825.

Williams, L.B., Hervig, R.L., Holloway, J.R., Hutcheon, I., 2001, Boron isotope geochemistry during diagenesis. Part I. Experimental determination of fractionation during illitization of smectite. Geochimica et Cosmochimica Acta, 65: 1769-1782.

Williams, L.B, and Hervig, R.L., 2004. Boron isotope composition of coals: a potential tracer of organic contaminated fluids. Applied Geochemistry 19: 1625-1636.

Wunder, B., Meixner, A., Romer, R.L., Wirth, R., Heinrich, W., 2005, The geochemical cycle of boron: Constraints from boron isotope partitioning experiments between mica and fluid. Lithos, 84: 206-216.

Zinner, E., Crozaz, G., 1986, A Method for the Quantitative Measurement of Rare Earth Elements in the Ion Microprobe, International Journal of Mass Spectrometry and Ion Processes, 69: 17-38.

APPENDIX A

PHLOGOPITE DATA COLLECTED AUGUST 2012—OCTOBER 2013

APPENDIX A

Sample Mount	Date	File Name	$\delta^{11}B$ corr.	$\delta^{11}B$ Int	Std. Err. Mean (%)	B ppm
		phlog* 1_1	23.3	23.3	0.07	
		phlog* 1_2	25.3	25.2	0.10	
		phlog 1_3	-3.8	-5.1	0.29	0.646
		phlog 1_4	13.0	13.0	0.05	10.780
		phlog 1_5	16.8	16.7	0.06	7.758
		phlog 1_6	21.2	21.4	0.08	6.040
		phlog 1_7	19.6	19.5	0.08	6.051
PTS-1_73-105		73-105 phlog 2_1	3.6	3.2	0.18	16.475
		73-105 phlog 2_2	6.5	5.8	0.20	3.094
		73-105 phlog 2_3	14.3	13.8	0.17	4.118
		73-105 phlog 2_4	11.0	11.3	0.18	4.018
	9/26-27/2012	73-105 phlog 2_5	8.8	8.4	0.15	4.525
		73-105_PHG_1	14.9	15.4	0.11	8.302
		73-105_PHG_2	4.5	4.2	0.17	3.165
		73-105_PHG_3	3.9	2.3	0.21	1.674
	5/15/13	73-105_PHG_4	16.3	16.3	0.08	9.797
		BT-7 PHG_1	7.6	8.5	0.38	1.829
PTS-2_BT-7		BT-7 PHG_2	12.7	11.1	0.42	0.273
		BT-7 PHG_3	13.9	14.9	0.32	0.538
	10/29/12	BT-7 PHG_4	8.0	9.0	0.28	0.451
		1359 PHG_1	7.2	10.4	0.50	0.407
		1359 PHG_2	-0.8	1.9	0.31	0.330
PTS-2_BD1359		1359 PHG_3	1.6	0.9	0.24	0.481
		1359 PHG_4	3.5	3.0	0.39	0.452
		1359 PHG_5	-10.0	-7.9	0.26	0.717
	10/29/12	1360 PHG_6	10.3	10.7	0.25	0.999
		RM@1	-11.5	-11.7	0.15	0.780
BD3130		RM@2	-9.6	-10.1	0.14	0.777
		RM@3	-8.0	-8.1	0.16	0.703
	8/30-31/12	RM@4	-9.8	-9.7	0.17	0.760
		PAL_ph_2	-11.6	-11.6	0.08	7.79
MGMt-3_PB_1		PAL_ph_3	-8.5	-8.5	0.11	8.85
		PAL_ph_4	-12.5	-12.5	0.11	8.52
	9/27/13	PAL_ph_5	-10.4	-10.4	0.09	8.86
		ROM-249_PH-01_1	-24.5	-25.0	0.25	0.585
		ROM-249_PH-01@1	-15.4	-15.7	0.18	0.791
MGMt-1_ROM249		ROM-249_PH-01@2	-23.0	-23.4	0.22	0.655
		ROM-249_PH-01@3	-9.0	-9.2	0.15	1.293
		ROM-249_PH-01@4	-4.5	-4.5	0.10	2.839
	2/22/13	ROM-249_PH-01_5	-9.8	-10.2	0.21	0.734
MGMt-2_BFT153	**4/18/13**	BFT-153_1	-14.81	-17.59	0.51	0.06
		104_1	-15.12	-15.30	0.25	0.606
		104_2a	-14.92	-14.78	0.40	0.513
		104_2b	-9.18	-9.66	0.38	0.645
MGMt-3_BFT104		104_3	-19.67	-19.91	0.16	0.713
		104_4	-22.09	-22.52	0.28	0.752
		104_5	-23.39	-23.26	0.21	0.519
	11/7/13	104_6	-19.72	-19.85	0.26	0.671
		BFT-297_1	-9.71	-10.67	0.24	0.230
	4/18/13	BFT-297_2	-1.97	-2.70	0.24	0.209

APPENDIX A

Sample Mount	Date	File Name	$\delta^{11}B$ corr.	$\delta^{11}B$ Int	Std. Err. Mean (%)	B ppm
MGMt-2_BFT297		BFT-297_1	-22.08	-22.75	0.18	0.270
		BFT-297@1	-24.76	-25.29	0.50	0.328
		BFT-297@2	-21.20	-21.88	0.18	0.293
	6/13/13	BFT-297@3	-24.74	-24.92	0.19	0.291
MGMt-2_BFT141a		141A_1	-22.94	-30.04	0.51	0.030
		141A_2	-2.49	-7.79	0.52	0.028
		141A@1	-16.19	-22.81	0.51	0.029
		141A@2	-9.46	-15.60	0.52	0.033
		141A@3	-21.41	-26.53	0.51	0.032
		141A@4	-5.59	-16.43	0.70	0.031
		141A@5	4.02	-8.37	0.71	0.034
		141A@6	-14.06	-23.30	0.59	0.050
		141A_8	-14.77	-17.74	1.52	0.048
	4/18/13	141A_9	-17.05	-16.14	0.53	0.048
Mt-168_BFT-405		BFT405 F_1	-38.96	-40.25	0.44	0.498
		BFT405 F@1	-22.30	-24.80	0.25	0.357
		BFT405 F@2	-20.17	-22.87	0.26	0.386
		BFT405 F@3	-21.66	-24.36	0.26	0.405
		BFT405 F@4	-19.59	-21.66	0.26	0.354
		BFT 405 E_1	-39.95	-40.45	0.32	0.451
		BFT 405 E@1	-16.07	-16.84	0.24	0.305
		BFT 405 E@2	-13.31	-14.14	0.23	0.348
		BFT 405 E@3	-15.89	-17.53	0.26	0.354
	10/25/12	BFT 405 E@4	-10.80	-11.20	0.22	0.405
Mt-168_BFT404		BFT 404 E_1	-32.32	-33.12	1.19	0.134
		BFT 404 E@1	-29.53	-31.51	0.47	0.088
		BFT 404 E@2	-21.78	-25.87	0.48	0.076
		BFT 404 E@3	-24.40	-28.12	0.50	0.078
		BFT 404 E@4	-9.11	-11.68	0.53	0.073
		BFT 404 E@5	-36.63	-36.73	0.60	0.060
		BFT 404 E@6	-19.70	-22.46	0.56	0.051
		BFT 404 E@7	-25.66	-25.30	0.45	0.098
	10/25/12	BFT 404 E@8	-24.74	-27.04	0.40	0.125
MGMt-1_MON 22		MON-22_1CT &@1	-28.65	-29.07	0.20	0.537
		MON-22_@2	-26.19	-26.82	0.23	0.450
		MON-22_@3	-31.25	-31.84	0.23	0.448
		MON-22_@4	-28.22	-28.85	0.22	0.464
		MON-22_@5	-28.64	-29.06	0.22	0.483
		MON-22_@6	-31.98	-32.71	0.24	0.459
		MON-22_@7	-31.76	-32.19	0.22	0.525
		MON-22_@8	-31.03	-31.80	0.23	0.478
		MON-22_@9	-26.95	-27.73	0.26	0.411
	2/22/13	MON-22_10	-29.98	-30.54	0.31	0.423
MGMt-2_BFT137		BFT-137_1	-39.66	-45.63	0.48	0.031
		BFT-137_2	-21.12	-7.45	0.34	0.129
	5/13/13	BFT-137_3	-36.76	-37.17	0.42	0.051
		BFT-137-2_1	-32.58	-40.21	0.82	0.025
		BFT-137-2_@1	-58.95	-62.83	0.45	0.038
		BFT-137-2_@2	-28.40	-30.97	0.49	0.025
		BFT-137-2_@3	-31.74	-36.53	0.54	0.024
		BFT-137-2_@4	-21.14	-23.42	0.54	0.029
		BFT-137-2_@5	-37.29	-40.36	0.52	0.024
		BFT-137-2_@6	-20.88	-22.35	0.47	0.029
		BFT-137-2_@7	-29.16	-31.72	0.46	0.035

APPENDIX A

Sample Mount	Date	File Name	$\delta^{11}B$ corr.	$\delta^{11}B$ Int	Std. Err. Mean (%)	B ppm
	6/13/13	BFT-137-2_@8	-20.96	-23.08	0.51	0.033
MGMt-2_BFT147	**4/18/13**	BFT-147-P1_1	-157.21	-202.52	4.17	0.004
MGMt-1_SanCar_1	**2/22/13**	SanCar_1	-4.60	-12.11	1.14	0.046

APPENDIX B

CLINOPYROXENE DATA COLLECTED DECEMBER 2012—APRIL 2014

APPENDIX B

Sample Mount	Date	Sample	$\delta^{11}B$ corr.	$\delta^{11}B$ Int	Std. Err. Mean (%)	B ppm
		ROM-270_CI-11_2				0.154
		ROM-270_CI-11_3	-15.4	-15.7	0.35	0.149
		ROM-270_CI-11_4	-7.6	-7.6	0.33	0.150
		ROM-270_CI-11_5	-9.0	-10.0	0.41	0.177
MGMt-1_ROM-270_CI-11	2/22/13	ROM-270_CI-11_6	-1.6	-2.2	0.40	0.158
		73-105_CPX_1	-26.0	-20.2	0.92	0.278
PTS-1_73-105	5/15/13	73-105_CPX_2	-16.4	-20.6	0.64	0.134
PTS-2_BD1359		1359 CPX_1	-12.7	-16.3	0.95	0.718
		PAL_cpx@1	-15.8	-16.3	0.27	1.001
		PAL_cpx@2	-12.0	-12.2	0.28	0.888
		PAL_cpx@3	-14.2	-14.7	0.27	0.896
MGMt-3_PB_1	9/27/13	PAL_cpx@4	-15.9	-16.3	0.26	0.895
		DI-16_1	-11.4	-14.3	0.51	0.530
	12/7/12	DI-16_2	-9.8	-10.0	0.35	
		ROM-271_DI-16_1				0.153
		ROM-271_DI-16@1	-4.0	-7.0	0.44	0.150
		ROM-271_DI-16@2	-14.3	-17.6	0.47	0.090
		ROM-271_DI-16@3	-7.8	-11.4	0.46	0.103
		ROM-271_DI-16@4	-0.6	-3.4	0.43	0.099
		ROM-271_DI-16@5	-3.3	-6.2	0.43	0.099
		ROM-271_DI-16@6	-14.0	-17.1	0.44	0.098
		ROM-271_DI-16@7	-18.7	-22.2	0.46	0.100
		ROM-271_DI-16@8	-1.4	-5.4	0.44	0.101
		ROM-271_DI-16@9	-5.3	-10.0	0.51	0.091
MGMt-1_ROM-271_DI-16	2/22/13	ROM-271_DI-16@10	-5.2	-8.8	0.50	0.097
	11/7/13	104_C_1	-16.9	-20.0	0.58	0.117
MGMt-3_BFT104		104_C_2	-23.5	-28.2	0.41	0.115
		104_C_3	-20.6	-21.2	0.43	0.103
		104_C_4	-22.4	-25.4	0.47	0.099
		DI-10_CT				0.489
		DI-10_1	-10.2	-10.6	0.86	0.193
		DI-10@1	-12.3	-12.0	0.40	0.208
		DI-10@2	-16.6	-16.1	0.43	0.255
		DI-10@3	-15.5	-14.1	0.45	0.282
		DI-10@4	-8.9	-10.8	0.46	0.332
Mt-182_DI-10	12/7/12	DI-10@5	-17.0	-18.3	0.44	0.409
		BFT 405 C_1	-10.4	-14.1	0.71	0.343
Mt-168	10/25/12	BFT 405 C_2	-11.4	-14.1	0.52	0.265
		BFT 404 D_1	-2.6	-3.2	0.98	0.536
		BFT 404 D@1	-13.5	-7.3	0.61	0.062

		BFT 404 D@2	-27.7	-21.8	0.65	0.049
Mt-168_BFT404	10/25/12	BFT 404 D@3	-27.1	-24.3	0.69	0.037
		LAC-236_1	-19.8	-26.9	0.76	0.063
		LAC-236_2	-12.8	-13.9	0.75	0.058
		LAC-236_3	-17.0	-19.9	0.74	0.084
		LAC-236_4	-12.6	-15.1	0.64	0.084
		LAC-236_5	-17.8	-19.9	0.65	0.068
		*LAC-236@1	-17.8	-19.9	0.65	0.066
		*LAC-236@2	-11.4	-12.5	0.58	0.069
		LAC-236@3	-12.6	-14.7	0.68	0.070
		LAC-236@4	-8.2	-22.7	0.77	0.066
LAC-236	4/1/14	LAC-236@5	-6.4	-12.1	0.84	0.066
		LAC-P_1	-23.3	-21.9	0.69	0.103
		LAC-P_2	-5.6	-8.4	1.24	0.124
LAC-P	4/2/14	LAC-P_3	-20.6	-24.1	1.48	0.111

APPENDIX C

SERPENTINE, GARNET, OLIVINE AND AMPHIBOLE DATA

COLLECTED AUGUST 2012—SEPTEMBER 2013

APPENDIX C

	Sample Mount	Date	File Name	$\delta^{11}B$ corr.	$\delta^{11}B$ Int	Std. Err. Mean (%)	B ppm
SERPENTINE		9/26/12	Serpentine	12.7		0.02	
	PTS-1_73-105		73-105_SERP_1	10.0	10.0	0.04	217
			73-105_SERP_2	18.0	18.0	0.04	189
			73-105_SERP_3	31.1	31.1	0.07	297
			73-105_SERP_4	13.1	13.1	0.05	72
		5/15/13	73-105_SERP_5	22.7	22.7	0.05	86
GARNET	PTS-1_73-105	9/26/12	Garnet	-10.3		0.79	
		5/15/13	73-105_GT-1	-26.6	-21.0	1.41	0.06
	MGMt-4_BFT405	9/25/13	405_gt_1	1.4	-8.9	1.16	0.40
	MGMt-4_BFT297	9/25/13	297_Gt_1	17.8	-4.6	1.49	0.01
OLIVINE	PTS-1_73-105	5/15/13	73-105_OL_1	-17.1	-20.5	0.42	0.19
	PTS-2_BT-7		BT-7@1	-20.1	-22.4	0.62	0.05
			BT-7@2	-20.6	-50.5	0.65	0.05
			BT-7@3	1.7	-7.2	0.40	0.09
			BT-7@4	-13.2	-19.9	0.48	0.07
		6/14/13	BT-7@5	-7.2	-13.7	0.47	0.09
AMPHIBOLE	BD3130		BD3130_1	-12.9	-12.9	0.18	0.9059
			BD 3130@1	-12.1	-12.2	0.15	0.9791
			BD 3130@2	-11.9	-11.9	0.12	0.9514
			BD 3130@3	-10.5	-10.6	0.14	0.9428
			BD 3130@4	-9.8	-9.9	0.15	0.9253
		8/30-31/12	BD 3130@5	-13.3	-13.4	0.14	0.9031